Decoding the steady elongational viscosity of monodisperse linear polymers using tube-based modeling

Céline Hannecart, Taisir Shahid, Dimitris Vlassopoulos, et al.

Citation: Journal of Rheology **66**, 197 (2022); doi: 10.1122/8.0000182
View online: https://doi.org/10.1122/8.0000182
View Table of Contents: https://sor.scitation.org/toc/jor/66/1
Published by the The Society of Rheology

Decoding the steady elongational viscosity of monodisperse linear polymers using tube-based modeling

Céline Hannecart,[1] Taisir Shahid,[1,2] Dimitris Vlassopoulos,[3,4] Filip Oosterlinck,[5] Christian Clasen,[2] and Evelyne van Ruymbeke[1,a)]

[1]*Bio and Soft Matter, Institute on Condensed Matter and Nano-science, Université Catholique de Louvain, Louvain-la-Neuve, Belgium*
[2]*Department of Chemical Engineering, KU Leuven, Celestijnenlaan 200f, 3001 Leuven, Belgium*
[3]*Foundation for Research and Technology—Hellas (F.O.R.T.H.), Institute of Electronic Structure and Laser, Heraklion, Crete, Greece*
[4]*Department of Materials Science and Technology, University of Crete, Heraklion, Crete, Greece*
[5]*DSM Materials Science Center, P.O. Box 18, NL-6160 MD Geleen, The Netherlands*

(Received 30 October 2020; final revision received 30 November 2021; published 29 December 2021)

Abstract

The current coarse-grained picture to represent polymer chain dynamics under uniaxial extensional flow (based on the Doi–Edwards model) fails to predict some scaling dependencies of material properties on deformation rate observed experimentally, specifically the monotonic thinning behavior of polymer melts. Recently, new mechanisms based on the concept of monomeric friction reduction have been proposed to explain this peculiar behavior; however, it is difficult to include them in the framework of the standard tube model. Therefore, in this work, we propose an alternative treatment which does not rule out friction reduction but uses a different approach. It considers that the chain can stretch up to a certain level that we determine based on the Pincus blob picture, in place of determining to which extend the chain stretch is reduced compared to its finite extensibility. To this end, we revisit the extensional rheological data of polystyrene melts and see how the specificities of chains under strong elongational flow can be integrated into a tube model. This requires accounting for possible flow-induced chain orientation, stretching, and disentanglement. In particular, we extend the picture of Pincus blobs and define different levels of stretch that a chain can reach as a function of the extensional rate by invoking a rate-dependent blob picture. While this approach requires introducing an additional parameter to describe the stretch relaxation time, the results are in good agreement with the experimental observations. This alternative but sound approach should contribute to the on-going discussion on the elongation of entangled polymers. © *2021 The Society of Rheology.* https://doi.org/10.1122/8.0000182

I. INTRODUCTION

Today, the linear viscoelastic (LVE) properties of monodisperse linear polymers are well understood and have been successfully described by mesoscopic models, such as tube models [1–8] or slip-link models [9–13], which allow to account for the effect of entanglements between chains. On the contrary, our present understanding of the dynamics of polymer melts under large deformation and, in particular, under uniaxial extension, has not reached the same level, and many fundamental questions still need to be addressed in order to be able to satisfactorily describe their nonlinear viscoelastic response [14–17]. More specifically, in the case of well-entangled monodisperse polymer melts ($Z > 10$), experimental steady viscosity data have shown a monotonic extensional thinning behavior [18] with no sign of an upturn even at strain rates larger than the reciprocal Rouse time of the chain [19]. This behavior was unexpected: As explained by Marrucci and Ianniruberto in [20,21], it was believed that at strain rates larger than the inverse Rouse time of the chain, i.e., at a Rouse–Weissenberg number Wi_R larger than 1, the chains stretch up to their finite extensibility, leading to a large and rapid increase of their steady elongation viscosity with strain rate, i.e., leading to a significant extension-rate thickening. In fact, such behavior was in good agreement with previously reported experimental steady viscosity data for entangled polymer solutions [22].

In recent years, the difference in behavior between polymer melts and solutions has been confirmed. It is now well-established from experimental studies [15,16,18,23–28] that, under strong elongational flow, the tensile stress growth coefficient of polymer melts exhibits transient strain hardening accompanied by an elongation thinning of the extensional viscosity η_E, which is well described by the scaling law $\eta_E \sim \dot{\varepsilon}^{-1/2}$, while an upturn of the extensional viscosity with increasing rate has been observed for polymer solutions containing the same number of entanglement segments [14–16,29–31]. The present tube models are unable to explain these qualitatively different behaviors within a single framework, and the microscopic picture that was previously proposed to describe the extensional viscosity needs to be revisited.

Recently, different new models have emerged that are based on novel mechanisms, in order to address the failure of

a)Author to whom correspondence should be addressed; electronic mail: evelyne.vanruymbeke@uclouvain.be

the initial tube model approach to describe the observed extensional thinning. The first proposed mechanism that could successfully explain this reduced steady viscosity in polymer melts was the interchain tube pressure (ICP) concept proposed by Marrucci and Ianniruberto [21]. According to this concept, a strong elongational deformation causes the tube to contract, thus decreasing the tube diameter with respect to its equilibrium value. As the tube diameter decreases, pressure starts to build up against the tube wall and after a while this growing pressure is sufficiently large to stop the contraction process, giving rise to a steady state. This concept, which ensures that the extensional viscosity scales with $\dot{\varepsilon}^{-1/2}$ at high rates, is still used today by the group of Wagner [32–37], who studied the elongation properties of polymer melts and solutions. Based on ICP as well as a new definition of the Rouse time of the chain under elongation, these authors could successfully describe the extensional viscosity of polymer chains in solution and in the melt state. However, this approach requires the tube diameter relaxation time to depend on the sample composition [32,33], which should not be the case since this time should only scale as the Rouse time of the chain [21,38]. Furthermore, since the tube-pressure concept cannot differentiate between polymer melts and solutions, two different Rouse times (for polymer melt and solution) must be used in order to describe the data [33–35].

Alternatively, several works have been proposed that are based on the idea that extensional thinning observed in the melt state originates from a reduction of the monomeric friction under fast extensional flow (Stretch/Orientation-induced Reduction of Friction, SORF concept) [39–41,44]. According to this approach, when the extensional flow is faster than the stretch relaxation rate, the local environment of the polymer deviates from its equilibrium state and becomes strongly anisotropic. This local anisotropy then leads to a decrease in monomeric friction and the corresponding stretch saturates at a lower level. Thus, this mechanism mainly affects the long chains and should be predominant for polymer melts, as the small solvent molecules in a solution do not align with the flow and remain isotropic. This concept has been successfully implemented for both polystyrene (PS) melts [17,39] and solutions [41–43]. However, in order to quantitatively describe the data, an additional parameter related to a possible nematic effect between the chains under elongation [45] must be taken into account [44], which raises new questions about the ability of this approach to predict the elongational viscosity over a large range of strain rates. Elongational properties of polymer melts have also been studied by bead-spring models. For example, O'Connor *et al.* [46] used Molecular Dynamics simulations based on a Kremer–Grest bead-spring model to model the viscoelastic response of linear chains under uniaxial elongation and succeeded in reproducing the experimental results very well. Bobbili and Milner [47] recently confirmed the friction reduction in flow by simulating polymer melts under elongational flow with bead-spring chains and purely repulsive interactions. They observed that the mean-squared bead displacement in the x-direction (i.e., the flow direction) increases for a chain submitted to a larger tension, i.e., its diffusion coefficient increases and thus its friction coefficient decreases. Since stretching the chains in the x-direction leads to an increase in the distance along the x-axis that a chain has to cover in order to renew its position, one could therefore explain the observed decrease in monomeric friction in the x-direction by a smaller number of "detours" the chain can make in the y- and z-directions.

By looking at the chain conformation as a function of the elongation rate, the work of O'Connor *et al.* [46] also showed that for $Wi_R > 1$ chain stretching depends on two factors, (1) the actual value of Wi_R and (2) the equilibrium number of Kuhn segments in an entanglement N_e, i.e., the chain flexibility, and consequently on the polymer chemistry [39]. This observation has been later confirmed experimentally by Matsumiya *et al.* [43,48], who found different stretching levels for unentangled PS and poly(ter-butylstyrene) (PtBS) melts. In that work, extension thickening followed by extension thinning was found for both samples. The authors explained the results by an effect of finite extensibility of the chain during the extension-thickening region and the suppression of this finite extensibility effect by monomeric friction reduction during the extension-thinning regime. The same data were recently modeled by Narimissa and Wagner [37] based on a phenomenological approach. They concluded that elongational thinning of these unentangled polymers at high Wi_R numbers was rather caused by a finite stretch in combination with strand orientation. By considering the maximum stretch as an adjustable parameter, the latter approach leads to a very good agreement with the experimental data. However, this approach still needs to be validated for entangled polymers. The role of the physico-chemical properties of the polymer on the elongation properties has also been shown by Morelly *et al.* [49], who studied the finite extensibility and stretching ability of PS, PtBS, and PMMA polymers.

A different approach was used by Schweizer and Sussman [50] who proposed that, similarly to rodlike polymers, polymer chains that are aligned in the flow direction can lead to an enlargement of the tube in which they are confined. These two conjectures have been tested by Desai and Larson [51], in combination with the Doi–Edwards–Marrucci–Grizzuti (DEMG) model [52], and compared with the experimental data. They concluded that both extension thinning in the melt state and extension thickening in solution can be captured by such an approach, under the condition that the chain friction varies with the stretch/orientation of the chains under flow. However, as suggested by the authors, the way the friction depends on the chain stretch is probably not universal.

From the above, it is evident that the origin of elongational thinning in polymer melts is still under discussion. In the present work, we would like to further contribute to the ongoing debate by analyzing the available experimental data for the tensile stress growth coefficient and the extensional viscosity of monodisperse polymer melts with the help of our tube-based Time-Marching Algorithm (TMA) [53–55]. Our objective is to start from our model and see how mechanisms such as reptation, contour length fluctuations (CLFs), or constraint release (CR), which are present in the linear regime, are affected by the nonlinear elongational flow. We also propose a new description of the chain stretch, which saturates before reaching a finite extensibility limit based on

a rate-dependent blob picture. In this approach, considering the friction reduction is therefore not necessary as the main consequence of this process is to limit the chain stretch, which is achieved here based on the Pincus blobs picture [56,57]. Furthermore, elongational thickening, which takes place at intermediate rates, can be thought of as a transition regime, where the CLF and CR mechanisms are gradually suppressed before the chains start to stretch. The microscopic picture that we propose in Sec. IV is based on three observations drawn from literature results:

(1) In the thinning regime, polymer chains are stretched at the level of the entanglement segments.

Following [58] and as usually done in the tube model, we assume that the stress can be calculated from the orientation distribution of occupied tube segments [8]. If the tube segments are not stretched beyond their equilibrium length, the stress tensor can be written as

$$\boldsymbol{\sigma} = \frac{15}{4} G_N^0 \langle \boldsymbol{uu} \rangle, \tag{1}$$

where $\boldsymbol{u}$ represents the normalized vector connecting neighboring entanglement segments and the brackets represent the average over the orientation distribution. This equation does not hold if the tube segments are stretched by a factor λ beyond their equilibrium length, i.e., $\lambda = l/l_0 = L/L_{eq} > 1$, with l and l_0 being the length and the equilibrium length of an entanglement segment, while L and L_{eq} are the length and the equilibrium length of the chain primitive path. In such a case, the number of occupied and oriented tube segments that contribute to the stress increases with λ, and the thermodynamic tension carried by the chain also grows with λ. Therefore, the stress is found to quadratically increase with λ,

$$\boldsymbol{\sigma} = \frac{15}{4} G_N^0 \boldsymbol{S} \lambda^2, \tag{2}$$

where $\boldsymbol{S}$ is the tube segments orientation tensor and λ is the stretch of an entanglement segment.

In case the entanglement segments are fully oriented in the flow direction but are not stretched beyond their equilibrium length (i.e., $\lambda = 1$), the tensile stress growth coefficient η_E^+, which is equal to $(\sigma_{zz} - \sigma_{rr})/\dot{\varepsilon}$, where σ_{zz} and σ_{rr} are the axial and the radial stress component and $\dot{\varepsilon}$ is the Hencky strain rate, reaches a steady value which is well approximated as $\eta_E = (15/4) G_N^0 \dot{\varepsilon}^{-1}$. This scaling exponent of -1 should be observed at strain rates larger than the inverse disentanglement time of the polymer melt, τ_d, but lower than its inverse Rouse time, τ_R [21]. Thus, a scaling exponent of $-1/2$ experimentally found at larger strain rates as discussed above (rather than an exponent of -1) suggests that in this case the chains are not only oriented but also stretched at the level of entanglement segments. A scaling exponent of $-1/2$ has been observed experimentally with different polymer chemistries and architectures [18,26,27], taking sometimes slightly different values in specific cases [49]. At very high rates, when the chains are approaching their finite extensibility limit, this scaling law should not be valid anymore [51].

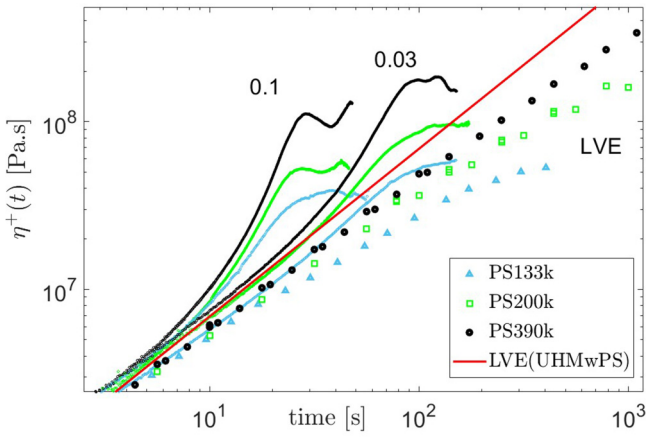

FIG. 1. Tensile stress growth coefficient versus time for the monodisperse polymer melts PS133 (light blue, ▲), PS200 (green, □), and PS390 (black, ○) at different extensional rates (in s^{-1}, indicated by the numbers). The red line corresponds to the theoretical linear envelop of a hypothetical UHMwPS, for which the relaxation time is assumed to be too long to be observed within the experimental time window. LVE data are given for comparison (indicated by "LVE"), data are taken from [16,18,24].

Chain stretching at the level of entanglement segments can also be observed in the transient elongation response of monodisperse polymer melts: as illustrated in Fig. 1, the corresponding tensile stress growth coefficient plotted as a function of time clearly starts to depart from the linear envelop at high extensional rates, exhibiting transient strain hardening. At high rates, this transient strain hardening exceeds the predicted linear envelop of a hypothetical ultrahigh molecular weight PS (hereafter called UHMwPS), characterized by a relaxation time much longer than the experimental time window [so that its LVE envelop (see the red line in Fig. 1) is well described by $|\eta^*(t)| = 3G_N^0 t$, with the plateau modulus $G_N^0 = 230\,\text{kPa}$ (see Sec. III B)]. The larger value of the tensile stress growth coefficient of the examined samples, compared to the linear response of this UHMwPS, can only be explained by considering that the chains are stretched at the level of entanglement segments, despite the elongational thinning observed as a function of the stretch rate.

(2) In the thinning regime, polymer chains reach a steady state but do not reach their finite extensibility.

While in some models [14,37], it is assumed that any chain that is elongated faster than its inverse Rouse time reaches its finite extensibility, recent works have shown that this is not the case. In particular, by comparing rheometric data on tensile stress growth coefficient and scattering data on chain orientation, Wingstrand *et al.* [59] showed that in strong flows the former can reach a steady state while the chains are not fully extended. They also showed that the maximum stretch state (i.e., the conformation of the stretched chains) reached by the chains depends on the imposed stretch rate. This result again suggests that in strong flows the chains do not fully stretch up to their finite extensibility, as if intermediate levels of stretch could exist. Similar results were also reported by Watanabe *et al.* [60] in the case of unentangled chains. Qin and Milner [61] based on Monte Carlo simulations. These authors demonstrated that the average

end-to-end distance in the direction of the elongation does not vary linearly with the tension anymore and is smaller than expected and below the finite extensibility limit. In this work, the chains are seen as a sequence of tension or Pincus [62] blobs aligned within the direction of the flow. Each of these tension blobs has Gaussian properties, while the trajectories of longer subchains were considered biased random walks since they are extended in the flow direction. The recent MD simulations of O'Connor *et al.* [46] also support this view. Indeed, the authors showed that by increasing the elongational rate, the chains are becoming straightened, but on progressively smaller length scales, leading to a saturation of the stretch before its finite extensibility limit.

(3) At large elongational rates, the steady-state regime of monodisperse linear entangled polymer melts of the same chemistry is fully governed by their Rouse time.

As also shown by O'Connor *et al.* [46] and earlier by Marrucci and Ianniruberto [21] and Bach *et al.* [23], in the steady regime, the stretch level of polymer chains of the same chemistry is only a function of Wi_R (based on their Rouse time) and increases with increasing Wi_R. This means that if finite extensibility is not reached at the same elongational rate and steady state, the entanglement segments of a long chain are more stretched than the entanglement segments of a shorter chain.

This is also observed in the experimental data of the tensile stress growth coefficient [16,18]. For example, Fig. 1 depicts tensile stress growth coefficient data of PS melts with different molar masses, but deformed at the same strain rates. These samples display a similar transient behavior; however, the respective data saturate at different levels, i.e., the stretch ratio λ of an entanglement segment in the steady-state regime increases with the length (molar mass) of the chains. In order to reach the same stretch level, different stretch rates should be used to ensure that the samples are deformed at the same Wi_R.

Furthermore, the work of Shahid *et al.* [63] showed that, based on their experimental results, the steady-state stretch state reached by entangled long chains blended with different shorter polymer matrices is independent of the molar mass of the matrix, thus independent of the orientation state of the latter. A similar conclusion was also drawn in [38], based on the PS blends proposed in [24]. Hence, these results are in agreement with the findings of O'Connor and co-workers, which suggest that, in the steady-state regime, the stretch state of a chain is only a function of Wi_R [46].

Inspired by these three observations, we further examine how the orientation and stretch state of the chains in the steady-state regime depend on their molar mass and on the extensional rate, and how the different thermal relaxation mechanisms such as reptation, CLFs, or CR are affected by a strong flow. Based on our analysis, we develop a simple model that is able to predict the extensional viscosity of linear polymer melts, without invoking additional relaxation mechanisms or finite extensibility criteria.

The paper is structured as follows: after the introduction, the linear polymers used in this work are briefly presented in Sec. II. Then, Sec. III introduces the LVE properties of these samples and their description with our tube model. In Sec. IV, the elongational properties of the samples are analyzed, and based on our observations a simple model is proposed to predict the steady and transient elongation properties of the samples. Finally, conclusions are presented in Sec. V.

TABLE I. Main characteristics of the pS melts used in this work.

Sample code	M_w (g/mol)	M_n (g/mol)	τ_R (at $T-T_g=23.4$ °C)	Ref.
PS27	27 100	26 500	1.8	50
PS50	51 700	50 380	6.5	24
PS100	102 800	100 600	25.8	24
PS133	133 000	131 600	43.2	16
PS185	185 000	179 600	83.7	6
PS200	200 000	192 000	97.8	18
PS285	285 000	261 500	198.6	15,29
PS390	390 000	367 000	371.8	18
PS545	545 000	486 600	726.1	15,29
PS820	820 000	803 900	1643	59

II. MONODISPERSE PS MELTS

In this study, we investigate the viscoelastic properties of a range of entangled monodisperse linear PS melts, which vary in molar mass. These samples have been studied in previous works [15,16,18,33], and their linear and nonlinear viscoelastic data have already been presented in the literature. They are listed in Table I, together with some basic physical characteristics. Their Rouse time, τ_R, has been determined from the TMA model (see Sec. IV A).

Due to the high activation energy of PS, it is essential to work under iso-T_g condition [65], to ensure that the storage and loss moduli of the samples superimpose well at high frequencies. While the viscoelastic data of the different samples measured at 130 °C showed a good superposition in this regime, a large shift of the data was found for the lowest Mw sample, PS27, which has a glass transition temperature lower than the $T_g = 106.6$ °C measured for the high Mw samples [64]. Consequently, both linear and nonlinear data of PS27 were shifted to ensure that the data are plotted at a constant $(T-T_g)$ value, equal to 23.4 °C. Since the glass transition temperature of sample PS27 is not known, a shift factor $a_T = 35$ (which corresponds to $T_g = 102$ °C for PS27—this sample was measured at 115 °C) was chosen in order to ensure a good superposition of the relaxation moduli at high frequency. To confirm this factor, the theoretical T_g of PS27 was calculated using the Fox–Flory equation: $T_g = T_{g,\infty} - (C/M)$, where $T_{g,\infty}$ is the glass temperature of a high molar mass polymer (for PS, $T_{g,\infty} = 106.6$ °C) and C is a constant depending on the polymer chemistry (for PS, $C = 1.1 \times 10^5$ g K/mol). For PS27, this would correspond to $T_g = 102.5$ °C, which is very close to the value obtained by manually fitting the data.

III. LVE PROPERTIES

A. Modeling

1. Original model

First, the LVE data are modeled, based on our TMA model. Details of the model can be found in [53–55] for the

case of linear chains. This model is based on three different material parameters: the plateau modulus G_N^0, the molecular weight between two entanglements $M_{e,0}$, and the Rouse relaxation time of an entanglement segment τ_e, where the plateau modulus G_N^0 is defined as

$$G_N^0 = \frac{4}{5}\frac{\rho RT}{M_{e,0}}, \tag{3}$$

with parameter ρ being the monomeric density, R being the gas constant, and T being the temperature.

In this model, the relaxation modulus $G(t)$ accounts for both the high frequency Rouse process, $G_R(t)$, and the disentanglement modulus $G_d(t)$,

$$G(t) = G_R(t) + G_d(t). \tag{4}$$

These moduli are expressed as

$$G_R(t) = \frac{\rho RT}{M}\left\{\frac{1}{5}\sum_{p=1}^{Z}\exp\left(-\frac{p^2 t}{\tau_R}\right) + \sum_{p=Z+1}^{N}\exp\left(-\frac{2p^2 t}{\tau_R}\right)\right\}, \tag{5}$$

$$G_d(t) = G_N^0\varphi(t)\{\Phi\}^{\alpha}. \tag{6}$$

In Eq. (5), τ_R represents the Rouse time of a chain with the weight-average molar mass M and containing Z entanglement segments, and N is the number of Kuhn segments in the chain. In Eq. (6), $\varphi(t)$ is the unrelaxed fraction of initial tube segments and, therefore, represents the fraction of tube segments, which are still oriented at time t. The exponent α is the dynamic dilution exponent, which is here fixed to 1, based on [64,66,67], where it was shown that for bidisperse polymer melts, the experimentally observed $\Phi^{4/3}$ scaling of the low-frequency plateau modulus was due to the loss of entanglements between two long chains induced by their monomeric tension equilibration. By accounting for this process, a good agreement was found between experimental and theoretical data, with $\alpha = 1$. In the case of monodisperse samples, the influence of tension equilibration is negligible. The function $\varphi(t)$ can be determined by looking at all molecular segments x, from $x = 0$ at the chain extremity to $x = 1$ in the middle, and by determining if these segments are still moving in their initial tube, i.e., by determining the probability that they have not yet relaxed through reptation or CLF mechanisms,

$$\varphi(t) = \int_0^1 \exp\left(\frac{-t}{\tau(x)}\right) dx, \tag{7}$$

with

$$\tau(x) = \left(\frac{1}{\tau_{\text{rept}}} + \frac{1}{\tau_{\text{fluc}}(x)}\right)^{-1}. \tag{8}$$

The reptation time, τ_{rept}, is equal to $3\tau_e(M/M_{e,0})^3$, while the fluctuation times are determined by taking into account both early fluctuations of the chain ends and the deeper, activated, retraction of the arms (considering it as a limiting two-arm star),

$$\tau_{\text{fluc}}(x) = \tau_{\text{early}}(x) = \frac{9\pi^3}{16}\tau_e\left(\frac{(M/2)}{M_{e,0}}\right)^4 x^4, \quad \text{for } x \le x_{tr}, \tag{9}$$

$$\ln(\tau_{\text{fluc}}(x)) = \ln(\tau_{\text{fluc}}(x-\delta x)) + 3\frac{(M/2)}{M_{e,0}}\, x\, \Phi(x)^{\alpha}\, \delta x, \quad \text{for } x > x_{tr}. \tag{10}$$

The position x_{tr} represents the position of the segment at which the retraction potential is equal to kT, i.e., at which the transition between early fluctuations and deep retraction is taking place. In order to calculate this retraction potential, it is considered in Eq. (10) that the molecular segment is located just before the segment x is positioned at $(x\text{-}\delta x)$. The function $\Phi(x)$ represents the polymer fraction that has not yet relaxed at the time the segment x of the arm is relaxing. This function is well approximated by $(1-x)$ since the samples are effectively monodisperse.

CR mechanisms are taken into account by the dilution factor $\Phi(t)$, which defines the effective diameter $a(t)$ of the dilating tube as $a(t) = a_0 \cdot \Phi(t)^{-\alpha/2}$, with a_0 being the initial tube diameter. Equivalently, $\Phi(t)$ represents the number of Gaussian blobs per segment of mass M_e. As long as the polymer relaxation takes place gradually, the dilution factor $\Phi(t)$ is equal to the unrelaxed fraction of initial tube segments, $\varphi(t)$ and evolves from 1 to 0 with the sample relaxation. However, this function cannot decrease faster than a Rouse process. Therefore,

$$\Phi(t+\delta t) = \max\left(\varphi(t+\delta t),\ \Phi(t)\sqrt{\frac{t}{t+\delta t}}\right). \tag{11}$$

In the case of the low molecular weight sample PS27, the relaxation modulus is determined by considering that the sample is unentangled. As shown in Sec. III B, its viscoelastic properties are well-described by considering that the chains relax by a full Rouse process. While the latter relaxation process is well-described by a discrete Rouse eigenvalues approach [68], we approximate it as

$$G(t) = \frac{\rho RT}{M}\sum_{p=1}^{n}\exp\left(-\frac{2p^2 t}{\tau_R}\right). \tag{12}$$

2. Simplified model

Despite the accuracy of the TMA model, it cannot be easily extended to the nonlinear regime because it considers an additive contribution of both Rouse and entanglement moduli in Eq. (4). Indeed, as further discussed in Sec. IV, since in the nonlinear regime entanglement segments can stretch, the continuity between the suppression of the CR process and the stretch region must be ensured. Therefore, $G_d(t)$ and $G_R(t)$ must be combined into a single equation

valid in the entire time domain. We propose here a simplified approach, which allows us to avoid adding the two contributions. In this model, the dilution factor $\Phi(t)$ is replaced by an effective "blob factor" $\Phi_{eff}(t)$, which corresponds to the diameter of the tube effectively explored by the chains. Thus, this factor has to account for the fact that, at short times, the chains need time to locally relax by a Rouse process. Consequently, at these short times, $\Phi_{eff}(t)$, which represents how many blobs with an orientation uncorrelated to their initial orientation an entanglement segment contains, can take values much larger than 1,

$$\Phi_{\text{eff}}(t) = \max\left(\varphi(t),\ \frac{5}{4}\sqrt{\frac{\tau_e}{2t}}\right). \tag{13}$$

With such a dilution factor, instead of Eq. (4), the relaxation modulus $G(t)$ is now defined as

$$G(t) = G_N^0\ \varphi(t)\Phi_{\text{eff}}(t). \tag{14}$$

The storage modulus $G'(\omega)$ and loss modulus $G''(\omega)$ are then determined from $G(t)$ by using the Schwarzl approximations [69], while the magnitude of the complex viscosity is determined from G' and G'',

$$|\eta^*(\omega)| = \frac{\sqrt{G'(\omega)^2 + G''(\omega)^2}}{\omega}. \tag{15}$$

A similar approach is followed for the unentangled PS27, in order to be able to include the stretch in this model, by simplifying Eq. (12) as

$$G(t) = \frac{5}{4}G_N^0 \exp\left(\frac{-2t}{\tau_R}\right)\sqrt{\frac{\tau_e}{2t}}, \quad \text{for } t > 0. \tag{16}$$

B. Comparison between theoretical and experimental data

The initial and simplified models presented in Sec. III A are used to predict the LVE response of the different monodisperse linear PS samples listed in Table I. This requires first to select the material parameters, which, referring to our previous works on PS samples [64,70,71], are set to 230 kPa and 15 kg mol^{-1} for G_N^0 and $M_{e,0}$, respectively, while τ_e has been set to 0.55 s at a reference temperature T such that $T - T_g = 23.4$ °C. As shown in Fig. 2, a good agreement is found between experimental and predicted data. The fact that the predicted curves for PS50 are less accurate is attributed to the weakly entangled state of the sample, at the limit of the validity of the tube picture. In this context, the experimental data with unentangled PS27 are not analyzed. We also observe that the storage and loss moduli predicted with the simplified model (dashed curves) are very close to those of the original (standard) model (shown by continuous curves). The main difference appears at relatively high frequencies and is due to the longitudinal Rouse modes, which are not accounted for in the simplified approach. In Fig. 3, the experimental complex viscosities are compared to the curves

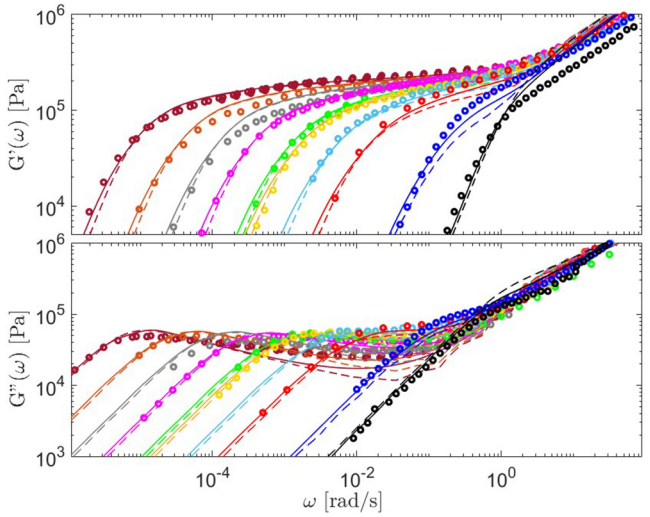

FIG. 2. Comparison between experimental (symbols) and theoretical (lines) storage and loss moduli of the different PS samples at $T - T_g = 23.4$ °C (from left to right: PS820, PS545, PS390, PS285, PS200, PS185, PS133, PS100, PS50, and PS27). Experimental data are taken from the literature (see Table I). The continuous curves correspond to the original (standard) TMA model, while the dashed curves correspond to the simplified approach (see the text).

predicted with the initial model (continuous curves) and the simplified model (dashed curves).

In the case of PS27, the use of the Rouse model [Eq. (12)] leads to a good agreement between the model and experimental data, while larger discrepancies appear with the simplified version. Nevertheless, even in this case, the predictions are accurate enough to be used for describing the extensional stress growth coefficient.

The good agreement found with the model gives a good starting point to analyze the extensional viscosity in the

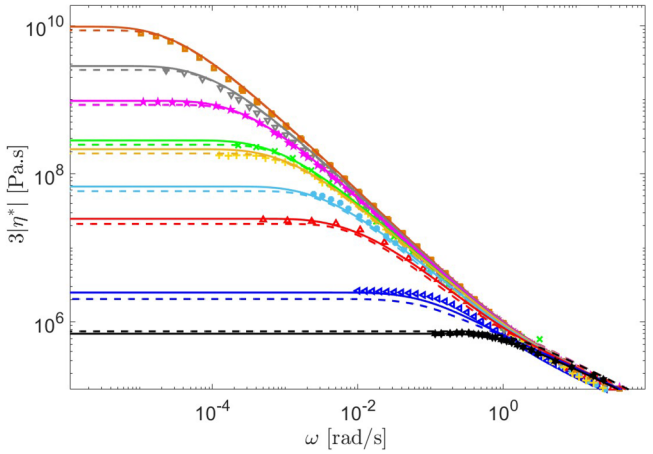

FIG. 3. Comparison between experimental (symbols) and theoretical (lines) magnitude of the complex viscosity of the different PS samples at $T - T_g = 23.4$ °C (from top to bottom: PS545, PS390, PS285, PS200, PS185, PS133, PS100, PS50, and PS27). For consistency with the other relevant figures, the complex viscosity $|\eta^*|$ has been multiplied by the Trouton ratio (equal to 3 for Newtonian liquids but also validated for polymers), which is a consequence of the assumption of incompressibility. Experimental data are taken from the literature (see Table I). The continuous curves correspond to the standard TMA model, while the dashed curves correspond to the simplified approach (see the text).

nonlinear regime. Furthermore, it validates the values chosen for the material parameters, which will be used to predict the nonlinear viscoelastic properties in Secs. IV A–IV C.

IV. NONLINEAR ELONGATIONAL PROPERTIES

Following an approach inspired by the Cox–Merz rule used with nonlinear shear flows [72], the extensional viscosities $\eta_E(\dot{\varepsilon})$ of the different polymers are first compared to their theoretical and experimental complex shear viscosities in the LVE regime, which have been multiplied by the Trouton ratio for uniaxial extension, $3|\eta^*(\omega)|$ [33]. We see in Fig. 4 that at low elongational rates the zero-rate viscosity follows the complex viscosity satisfactorily, while at higher strain rates the extensional viscosity is well above the linear response $3|\eta^*(\omega)|$, which represents (within a numerical factor) the extensional viscosity predicted by the Doi–Edwards model [8]. As discussed in Sec. I, this deviation appears as soon as strain hardening kicks-in during the transient response of the polymer melt under elongation.

As already mentioned, a scaling law [$\eta_E(\dot{\varepsilon}) \propto \dot{\varepsilon}^{-1/2}$] is found for most of the samples at large elongation rates (see also Fig. 7). This $-1/2$ dependence appears once the steady tensile stress growth coefficient exceeds the limit set by the black line determined by considering $|G^*(\omega)| = G_N^0$, i.e., corresponding to the case of polymer chains with fully oriented (albeit not stretched) entanglement segments. $|G^*(\omega)| = G_N^0$ also corresponds to the linear response of the hypothetical UHMwPS (introduced in Fig. 1) after the Rouse relaxation of its entanglement segments τ_e and before its relaxation by reptation or CLF. Thus, as soon as the extensional viscosity values of the polymer melts exceed this limit, the entanglement segments of the polymer chains are necessarily stretched. It should be noted here that the complex viscosity curve of the hypothetical UHMwPS is comparable (within a numerical factor of 5/4) to the response of the Doi–Edwards model without independent alignment for an entangled polymer melts at large strain rates [see Eq. (1)] [8].

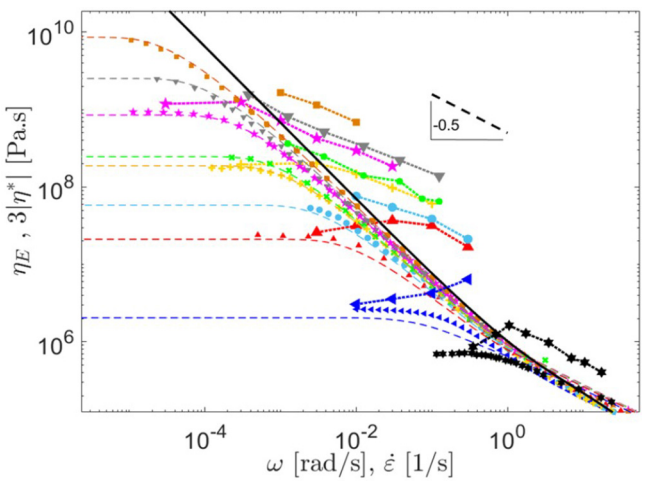

FIG. 4. Extensional viscosity versus elongational rate. Comparison between experimental data of PS545 (■), PS390 (▼), PS285 (*), PS200 (●), PS185 (+), PS133 (●), PS100 (▲), PS50 (◀), and PS27(*) at $T - T_g = 23.4$ °C, with theoretical predictions assuming that the chains are not stretched. The thick black line represents $3|\eta^*|$ of a hypothetical UHMwPS.

In Sec. IV A, we first discuss the evolution of the stretch at the level of the entanglement segments. In Sec. IV B, we modify our tube model to predict that steady response first at high strain rates, i.e., $\dot{\varepsilon} > 1/\tau_R$, and then in the transition regime, which takes place between the linear and the large strain rate regimes. In Sec. IV C, we apply the modifications proposed in Sec. IV B to the approximate differential model of McLeish and Larson [58] to model the transient elongation response of the PS melts.

A. Stretch state of the entanglement segments under large strain rates ($\dot{\varepsilon} > 1/\tau_R$)

At large elongational rates ($\dot{\varepsilon} > 1/\tau_R$), the chains are stretched at the level of the entanglement segments [18,24,25]. This latter (or equivalently, the primitive path of the chain) should thus be nearly fully oriented. Assuming they are fully oriented, the stretch evolution of an entanglement segment belonging to a chain with a Rouse time τ_R (or equivalently, the stretch evolution of its primitive path length) can be described as [25,32,38,58]

$$\frac{d\lambda}{dt} = \lambda\dot{\varepsilon} - \frac{\lambda - 1}{\tau_R}, \tag{17}$$

where the stretch evolution is balanced by the stretch relaxation following a Rouse process. According to this equation, the stretch of an entanglement segment can only relax by the longest Rouse mode of the chain. Therefore, as soon as the strain rate is slightly faster than $1/\tau_R$, this leads to an unbounded increase in the stretch, which is then only limited by the finite extensibility of the entanglement segment defined as $\lambda_{\max} = N_e b/\sqrt{N_e} b = \sqrt{N_e}$ (where N_e is the number of Kuhn segments in an entanglement segment and b is the length of a Kuhn segment). Consequently, the tension in the chain is increasing fast. However, the experimental steady tensile stress growth coefficient does not show this large increase at rates above $1/\tau_R$ (see Fig. 1) and exhibits a steady-state (extensional viscosity) value decreasing with $\dot{\varepsilon}^{-1/2}$ (see Fig. 4). This suggests that in the steady-state regime at strain rates larger than $1/\tau_R$, but not large enough to approach the finite extensibility, the chains can partially relax their stretch. This situation can be compared to the stretch relaxation of polymer chain to which a large step deformation (such that the chain is fully stretched) is imposed and which can relax during a time period $t = 1/\dot{\varepsilon}$: the deformed chain needs a time of the order of τ_R to fully recover their initial equilibrium length; however, after a shorter time period, part of its stretch is relaxed and the contour length of the chain reaches a length $L > L_{\text{eq}}$, which depends on the time elapsed after the deformation step [8,73]. This relaxation scales with $t^{1/2}$ (i.e., with $1/\sqrt{\dot{\varepsilon}}$ since we look at the stretch state of a chain relaxing during a time period $t = 1/\dot{\varepsilon}$) as it involves the relaxation of all Rouse modes. This approach was already discussed by Colby *et al.* [56] for unentangled flexible polymer liquids under shear, for which it was shown that the Rouse model naturally leads to shear thinning upon a change in conformation. In their approach, they considered that only the Rouse modes

corresponding to sections of chain relaxing faster than the inverse deformation rate are not stretched, and are able to relax and dissipate energy: Thus, the stretched polymer chain can be seen as a linear array of internally equilibrated Pincus blobs whose size is determined by the longest mode able to dissipate energy, and which corresponds to the largest scale for which chain conformation remains unperturbed. A more detailed discussion of the blob picture for entangled chains in strong shear flow is presented in [74].

Therefore, we propose to take into account the contribution of all Rouse modes to the stretch relaxation: instead of a single mode acting against the chain stretch induced by the flow, we consider the action of all Rouse modes, which leads to a partial stretch relaxation under a constant Hencky strain rate. To this end, we first define the main stretch relaxation time $\tau_{\lambda,\mathrm{ent}}$ of an entanglement segment in a chain of molar mass M. In the stretch evolution of Eq. (17), this time should be proportional to the Rouse time of the chain [58], consistently with [46–49]

$$\tau_{\lambda,\mathrm{ent}} = \theta\tau_R, \tag{18}$$

with θ being a constant that should only depend on the sample chemistry and flexibility. While θ is expected to be equal to 1, a value of 3.1 is found here (see Sec. IV B). This constant probably depends on the different friction coefficients of the polymer chains of different chemistry, but it should not depend on the sample molar mass distribution. As discussed in Sec. I, the way θ depends on the sample chemistry is not clear and should be further investigated; however, this parameter should be related to N_e, the number of Kuhn segments in an entanglement segment [30]. The fact that under uniaxial extension, the relaxation time of an entanglement segment rather depends on τ_{Rouse} and not on τ_e as in the linear regime has been already addressed (see Sec. I). This suggests that the equilibration of an entanglement segment requires monomer movement along the entire chain backbone and cannot take place locally anymore.

In order to account for possible partial stretch relaxation, we consider that the Rouse mode p_{ent} (with $\tau_{\lambda,p} = \tau_{\lambda,\mathrm{ent}}/p_{\mathrm{ent}}^2$) also contributes to the relaxation of the stretched entanglement segments, but only down to the length $l_p = \sqrt{p_{\mathrm{ent}} N_e b^2}$.

Accounting for these different modes in Eq. (17) leads to a new differential equation describing the stretch evolution of a fully oriented entanglement segment (see Appendix A),

$$\frac{d\lambda}{dt} = \lambda\dot{\varepsilon} - \frac{\lambda - \sqrt{\lfloor\lambda^2\rfloor}}{\tau_{\lambda,\mathrm{ent}}/\lfloor\lambda^2\rfloor^2} - \sum_{p=1}^{\lfloor\lambda^2\rfloor-1} \frac{\sqrt{p+1}-\sqrt{p}}{\tau_{\lambda,\mathrm{ent}}/p^2}, \tag{19}$$

with $\lfloor\lambda^2\rfloor$ being the largest integer below λ^2. The main difference between Eqs. (19) and (17) is the way they converge at long times. Indeed, at high rates of deformation, Eq. (19) tends to a finite limit that reduces to (see Appendix B)

$$\lambda_{\mathrm{st}}(\dot{\varepsilon})^2 \approx \sqrt{5\tau_{\lambda,\mathrm{ent}}\dot{\varepsilon}}, \tag{20}$$

where $\lambda_{\mathrm{st}}(\dot{\varepsilon})$ is the stretch level of an entanglement segment reached in the steady regime of deformation. As evidenced from Eq. (19), at larger values of the stretch rate in the steady-state regime, the stretch state of an entanglement segment increases with the number of those Rouse modes that are too slow to relax. The longest mode $p_{\mathrm{eq,ent}}$ that can contribute to its stretch relaxation is $t_{l,p} = 1/\dot{\varepsilon}$ or, equivalently,

$$p_{\mathrm{eq,ent}} = \sqrt{\tau_{\lambda,\mathrm{ent}}\,\dot{\varepsilon}} = \sqrt{\theta\tau_R\dot{\varepsilon}}. \tag{21}$$

The above expression is in good agreement with Eq. (20) since λ_{st}^2 is the average of $p_{\mathrm{eq,ent}}$ for the whole sample over the time period from $t = 0$ to $t = 1/\dot{\varepsilon}$; thus, $\lambda_{\mathrm{st}}(\dot{\varepsilon})^2 = \dot{\varepsilon}\int_0^{1/\dot{\varepsilon}} \sqrt{(\tau_{\lambda,\mathrm{ent}}/t)}\,dt = 2\sqrt{\tau_{\lambda,\mathrm{ent}}\dot{\varepsilon}}$, i.e., a factor 1.1 lower than in Eq. (20). While Eq. (21) is used to determine the value of the steady-state elongational viscosity (see Sec. IV B), the extensional stress growth coefficient is determined based on the model of McLeish and Larson and, therefore, their steady stretch value rather corresponds to Eq. (20) (see Sec. IV C).

B. Predicting the extensional steady viscosity $\eta_E(\dot{\varepsilon})$ by means of tube-based modeling

1. $\eta_E(\dot{\varepsilon})$ under large strain rates ($\dot{\varepsilon} > 1/\tau_R$)

In order to predict the steady-state elongational viscosity with our tube-based model, we have to modify it to account for the possible stretch of the entanglement segments. To this end, we consider the chains deformed in the steady-state regime and determine what are their disentanglement and stretch states under these specific conditions. This allows us to determine the corresponding relaxation modulus, $G_{\dot{\varepsilon}}(t)$, which is then used to calculate the steady-state elongational viscosity. It must be noted that this approach, which has been used under shear flow in [75], is only valid in the steady-state regime and cannot be used to describe the time evolution of the extensional viscosity, since at shorter times, the apparent relaxation modulus is not equal to our "model-specific" $G_{\dot{\varepsilon}}(t)$.

As described in Sec. IV A and illustrated in the cartoon of Fig. 5, if the modes 1, 2,…, $p_{\mathrm{eq,ent}}$ are too slow to equilibrate under a strong elongational flow [i.e., $(\tau_{\lambda,\mathrm{ent}}/p^2) \geq (1/\dot{\varepsilon})$ with $p = 1, 2, \ldots, p_{\mathrm{eq,ent}}$], the corresponding terms in Eq. (19) are not decreasing fast enough to compensate the flow-induced stretch of the entanglement segments. Consequently, the stretch is increasing with time, up to a level equal to $\lambda_{\mathrm{st}}(\dot{\varepsilon})$ [see Eq. (20)], corresponding to a situation at which an entanglement segment is composed of $p_{\mathrm{eq,ent}}$ Pincus blobs of mass $M_{\lambda,\mathrm{eff}} = M_{e,0}/p_{\mathrm{eq,ent}}$ aligned in the flow direction [62]. This implies that the entanglement segments are not described by a random walk of Kuhn segments anymore, but rather contain $p_{\mathrm{eq,ent}}$ "internally equilibrated" but not "mutually equilibrated" small tension blobs. On the other hand, the larger relaxation modes ($p > p_{\mathrm{eq,ent}}$) are relaxing faster than the stretch evolution induced by the flow, therefore ensuring that the stretch does not increase above $\lambda_{\mathrm{st}}(\dot{\varepsilon})$.

Therefore, in order to include this effect in our tube model, we consider that the effective blob factor $\Phi_{\mathrm{eff},\,\dot{\varepsilon}}(t)$ [previously described by Eq. (13)] must also account for the

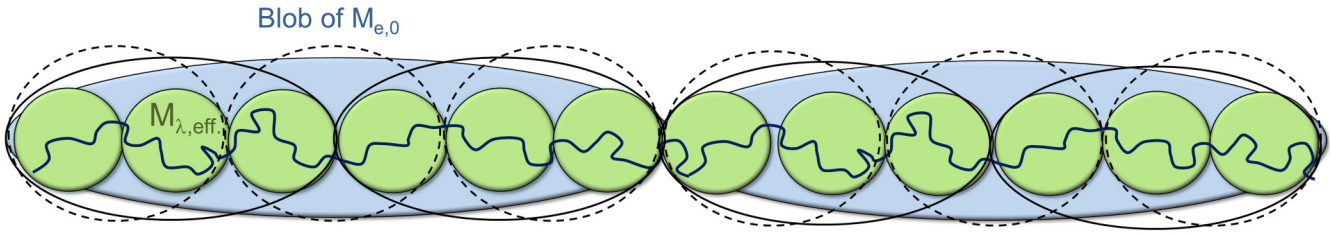

FIG. 5. Cartoon illustrating the stretch state of an entanglement segment at the steady-state regime (for a cartoon of the chain at equilibrium, see Fig. 10). In this specific case, $\Phi_\lambda(\dot{\varepsilon}) = p_{eq,ent} = 6$ (and $\lambda = \sqrt{6}$) since the stretch relaxation modes 1, 2,…, 6 are too slow to relax. The thin continuous and dashed curves in black represent modes 2 and 3, respectively.

reduction of the size of the internally equilibrated blobs due to the stretch of the entanglement segments. While in the linear regime, the size of these blobs only depends on the time the segments have to explore their surrounding by the Rouse process and then, at longer times, by the CR process, we now impose a condition that in the nonlinear regime the blob factor must be at least equal to $\Phi_\lambda(\dot{\varepsilon})$ $(= \lambda_{st}(\dot{\varepsilon})^2 \approx p_{eq,ent})$, which represents the number of internally equilibrated blobs within an entanglement segment. In the stretch regime, $\Phi_\lambda(\dot{\varepsilon})$ is larger than 1; therefore, this extra condition on the size of the internally equilibrated blobs can be seen as a "compression" of the effective tube within which the chain is moving. Indeed, the distance a_λ that the stretched chain can explore laterally is $a_\lambda = a_0 \cdot \lambda_{st}(\dot{\varepsilon})^{-1} = a_0 \cdot \Phi_l^{-1/2}$.

Considering the CR mechanism (which leads to a dilution of the effective tube diameter), the Rouse limitations at short time (which make the effective tube diameter increase from the length of a Kuhn segment b at time τ_0 to the length of an entanglement segment $\sqrt{N_e}b$ at time τ_e), and the possible stretch of the entanglements, we then consider that the effective blob factor $\Phi_{eff,\dot{\varepsilon}}(t)$, which represents the number of internally equilibrated blobs that a chain can explore during a time period t and under a strain rate $\dot{\varepsilon}$, is

$$\Phi_{eff,\dot{\varepsilon}}(t) = \max\left(\varphi(t),\ \frac{5}{4}\sqrt{\frac{\tau_e}{2t}},\ \Phi_\lambda(\dot{\varepsilon})\right). \tag{22}$$

It is noted here that, in the large strain rate regime ($\dot{\varepsilon} > 1/\tau_R$) at steady state, the latter expression could be simplified since the entanglement segments are fully oriented, i.e., reptation and CLF processes are not taking place, and thus, φ should be equal to *1*. This is not the case here since the expression of φ(t) is determined by assuming that the flow does not influence the reptation and CLF times. Nevertheless, this approximation, which is further discussed and corrected in Sec. IV B 2, has a negligible effect on the steady viscosity in the large strain rate regime since in this regime, $\Phi_{eff,\dot{\varepsilon}}(t)$ is governed by $\Phi_\lambda(\dot{\varepsilon})$, while the lifetime of an entanglement is governed by the convective CR process [see Eq. (24)]. As discussed below, Eq. (22) has the advantage of being applicable in the steady regime at any strain rate, from the linear regime toward the regime where the chains are stretched.

Based on Eq. (22), the corresponding steady-state extensional viscosity can be determined,

$$\eta_E(\dot{\varepsilon}) = \int_0^\infty G_{\dot{\varepsilon}}(t)dt = \int_0^\infty 3\ G_N^0\ \varphi(t)\Phi_C(t)\ \Phi_{eff,\dot{\varepsilon}}(t)\ dt. \tag{23}$$

In this equation, $G_{\dot{\varepsilon}}(t)$ represents the steady-state relaxation modulus determined by the tube model, while accounting for the influence of stretch on the tube diameter [through the function $\Phi_{eff,\dot{\varepsilon}}(t)$] and for the possible convective CR, described by the function $\Phi_C(t)$. As described in [21], this term accounts for obstacles being continuously removed in proportion to $\dot{\varepsilon}$ [76,77]. Therefore, the disentanglement time of a chain cannot exceed $1/\dot{\varepsilon}$,

$$\Phi_C(t) = \exp\left(\frac{-t}{\frac{1}{\dot{\varepsilon}}}\right). \tag{24}$$

Similarly, instead of using the convection term, the upper limit of the time integral can be set to $t = 1/\dot{\varepsilon}$ rather than infinite.

The steady-state extensional viscosities determined based on Eqs. (22)–(24) are shown in Fig. 6, and compared to the experimental data, for all samples apart from PS27, which will be discussed later. The constant θ in Eq. (18) was set to

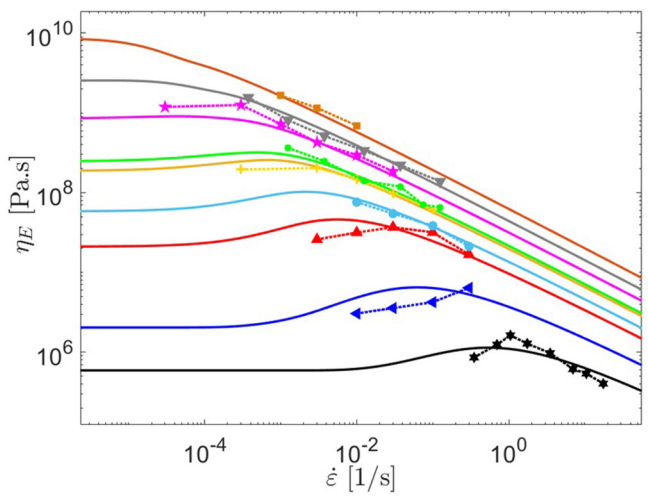

FIG. 6. Extensional viscosity versus elongational rate. Comparison between experimental data (o) of PS545 (■), PS390 (▼), PS285 (*), PS200 (●), PS185 (+), PS133 (●), PS100 (▲), PS50 (◀), and PS27 (*) at $T - T_g = 23.4$ °C, and theoretical predictions based on Eqs. (20)–(23), i.e., by assuming that the chains are fully oriented and that the stretch level of an entanglement blob saturated to $\lambda_{st}(\dot{\varepsilon})$. The parameter θ has been fixed to 3.1.

3.1 by a best-fit procedure, which is very close to the value of 3 found by Wagner and Rolon-Garrido [78]. As already mentioned, this constant is expected to depend on the chain flexibility and thus on the nature of the chain, but does not depend on the chain molar mass or the stretch rate [46,49]. However, since only one chemistry has been investigated in this work, no conclusion can be drawn on the value of this constant or its variance. A very good agreement is found for the different samples at large elongational rates. This result suggests that accounting for partial stretch relaxation provides a physically meaningful ingredient to capture the experimental data in the steady-state regime at a large stretch rate.

In the large deformation rate regime ($Wi_R > 1$, but below the finite extensibility limit), the chains can be considered fully oriented, which allows to approximate Eq. (23) as

$$\eta_E(\dot{\varepsilon}) = \int_0^\infty G_{\dot{\varepsilon}}(t)dt \approx 3G_N^0 \int_0^\infty \Phi_C(t)\Phi_\lambda(\dot{\varepsilon})dt = 3G_N^0 \frac{1}{\dot{\varepsilon}} 2\sqrt{\theta\tau_R\dot{\varepsilon}}. \quad (25)$$

This expression is very similar to the result of Marrucci and Ianniruberto, based on their interchain pressure concept [21], despite the different approach used in the present work and the different description of the stretch evolution [Eq. (19)]. In particular, while their approach considers that under large strain rates, the chain stretch does not reach finite extensibility in the steady regime because it is limited by the flow-induced pressure exerted by the chain against the tube wall, the present approach considers that the steady stretch saturates before reaching the FENE limit due to the internal equilibration of the monomer tension, which can take place up to a certain level depending on $\dot{\varepsilon}$. The difference between the two approaches is expected to be more pronounced by looking at the viscoelastic response of binary blends, for which the influence of the dynamic tube dilution (DTD) process is more important [38].

It is also similar to the prediction of Nielsen *et al.* [24], who used the model of Wiest. The key point of these similar, albeit differently derived expressions for the extensional viscosity is the same scaling at large rates, i.e., the power-law dependence with an exponent of $-1/2$.

This scaling [Eq. (25)] is validated in Fig. 7, where the extensional viscosities of the different samples are normalized by their respective molar masses. It is observed that indeed all data collapse on the same line, which corresponds to Eq. (25). Only sample PS50 does not appear to be deformed fast enough to reach this limit. This result highlights the experimental observation that at high rates the extensional viscosity should scale with $M\dot{\varepsilon}^{-(1/2)}$, as first described for PS in [23].

Therefore, despite the fact that some data exhibit low-rate elongational thickening [24] (see Fig. 11), it is possible to rationalize their high-stretch rate behavior as soon as the entanglement segments are fully oriented and stretched at a steady state.

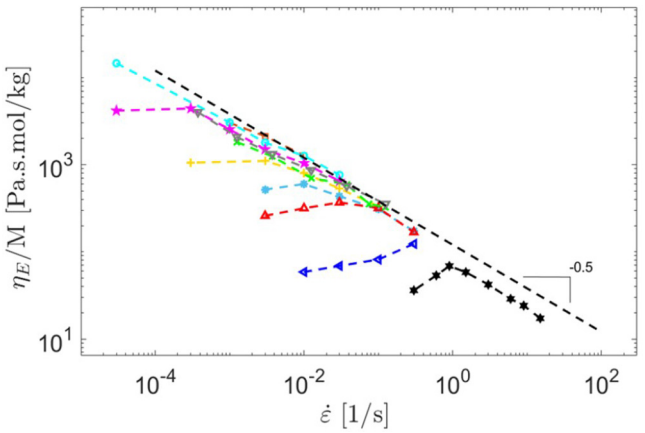

FIG. 7. Extensional viscosity normalized by the molar mass M of each sample versus uniaxial extensional rate. The symbols are the experimental data of PS545 (o), PS390 (▼), PS285 (*), PS200 (x), PS185 (+), PS133 (●), PS100 (▲), PS50 (◀), and PS27(*) at $T - T_g = 23.4$ °C. The dashed line corresponds to the expression of Eq. (25), i.e., $3G_N^0[(2\sqrt{\theta\tau_R\dot{\varepsilon}})/(M\dot{\varepsilon})]$.

2. $\eta_E(\dot{\varepsilon})$ in the transition regime of stretch rates ($1/\tau_d < \dot{\varepsilon} < 1/\tau_R$)

As observed in Fig. 4, the extensional viscosity data in the quasi-linear regime are well-described with the TMA LVE model [Eqs. (7)–(14)], and the same model applied to high elongational rates in Fig. 6 describes satisfyingly the data as well, by assuming that the entanglement segments are fully oriented and reach a steady-state stretch level, which depends on the number of Rouse modes that cannot relax fast enough. However, this approach fails to describe the transitional regime between the linear ($\dot{\varepsilon} < 1/\tau_d$) and the stretched ($\dot{\varepsilon} > 1/\tau_R$) regimes. This can be readily understood as follows: in the transitional regime, the molecules start to orient in the flow direction and the degree of orientation should increase with the elongational rate. Therefore, our initial assumption, according to which the tube representing the entanglement state of the chain is fully oriented, is not yet valid and must be corrected.

The importance of accounting for chain orientation is confirmed by looking at the tensile stress growth coefficient, as illustrated in Fig. 8. The transient hardening is already observed in this intermediate regime, despite the fact that the entanglement segments are not stretched ($\dot{\varepsilon} < 1/\tau_R$). In fact, in this regime, the strain hardening (see the orange diamonds in Fig. 8) occurs below the LVE envelop $|\eta^*_{\mathrm{UHMwPS}}(t)| = 3G_N^0 t$, which corresponds to a hypothetical UHMwPS with a relaxation modulus $G(t) = G_N^0$ within the experimental time window. This situation differs from the high stretch rate regime, where the transient strain hardening occurs above the $3G_N^0 t$ line (see the brown squares in Fig. 8). This suggests that the transient hardening at intermediate strain rates ($1/\tau_d < \dot{\varepsilon} < 1/\tau_R$) appears at a time $t = t_{\mathrm{onset}}$, at which the chains had already the time to partially relax by CLF and, consequently, by a CR process. In other words, at t_{onset}, the chains had time to partially disorient and the fraction of survival tube segments $\varphi(t_{\mathrm{onset}})$ as well as the effective dilution factor $\Phi_{\mathrm{eff},\dot{\varepsilon}}(t_{\mathrm{onset}})$ are lower than 1. At time $t > t_{\mathrm{onset}}$, while in the linear regime of deformation, the chains response

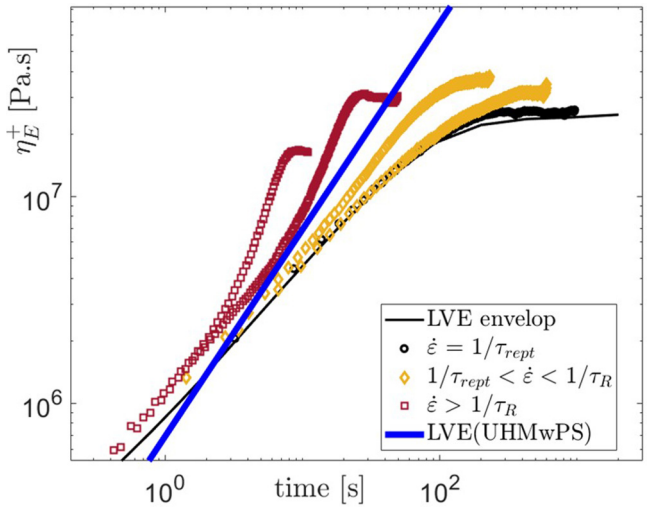

FIG. 8. Tensile stress growth coefficient (symbols) of PS100 with corresponding LVE envelop (black curve) and the linear envelop of a hypothetical UHMwPS sample (blue line) at $\dot{\varepsilon} = 0.3,\ 0.1,\ 0.03,\ 0.01,\ 0.003\,s^{-1}$ (from left to right). The data are taken from [24]. Note that $1/\tau_R \sim 0.04\,s^{-1}$ and $\tau_{rept} = 534$ s (at $T - T_g = 23.4$ °C).

further deviates from the $3G_N^0 t$ line due to the relaxation by CLF of the deeper chain segments before reaching their steady state, in the nonlinear regime, the relaxation by CLF stops and strain hardening is observed, which suggests that the relaxation by CLF of these deeper segments cannot take place. Therefore, the observed strain hardening, which does not come from the stretch of the entanglement segments, is attributed to a reduced effect of CLF and CR in comparison to the linear regime. This is linked to flow-induced orientation (or to be more exact, to a flow-induced reduced disorientation) of the entanglement segments rather than to their stretch. In the context of the tube model, it is therefore important to account for the influence of the elongational flow on the tube relaxation/disorientation [i.e., on $\varphi(t)$] in addition to its influence on the DTD process [79] [i.e., on $\Phi_{\text{eff},\dot{\varepsilon}}(t)$], as detailed below.

a. Flow-induced orientation of the entanglement segments. It is observed in Fig. 8 that at low strain rates (black data points) in the quasi-linear regime, the tensile stress growth coefficient first follows the LVE envelop of the unrelaxed UHMwPS (black line), but rapidly deviates from this curve to attain lower values well before reaching steady state. This deviation can be attributed to a partial relaxation of the chain by CLFs. At intermediate rates (orange data points in Fig. 8) the situation is different: while at short times the viscosity curve deviates from the LVE envelop of the unrelaxed UHMwPS sample in a similar way, CLF seems to be less efficient, leading to a lower decrease in the viscosity. We attribute this effect to the applied elongational rate, which does not allow the tube to relax by CLFs as much as in the linear regime: as illustrated in Fig. 9, at a given time period, random motions of the free chain ends can only take place if their corresponding fluctuation times are shorter than $1/\dot{\varepsilon}$; furthermore, these fast fluctuations will cover a shorter distance along the curvilinear tube axis if the latter is oriented. Hence, the flow-induced orientation of the tube segments reduces the contribution of CLFs, and the corresponding tensile stress growth coefficients are above the linear envelop. This leads to an "orientation-induced elongational-rate thickening": at intermediate strain rates ($1/\tau_d < \dot{\varepsilon} < 1/\tau_R$), the tube is not stretched, yet it cannot relax as easily as in the linear regime.

With increasing elongational rate, we expect that the tube becomes more and more oriented, yielding a gradual suppression of the relaxation of the tube segments by CLFs, thus a reduction of energy dissipation. Furthermore, since the importance of the CLF process increases with decreasing molar mass of the polymer chains, we expect that this "orientation-induced elongational rate thickening" becomes more significant with weakly entangled chains. This is indeed the case, as the experimental data indicate elongational thickening with low molar mass samples (especially for PS50 and PS100 samples in the present work).

In order to account for this gradual suppression of CLFs, we modify the corresponding early fluctuation times [see Eq. (9)], which is the main relaxation process of the linear chains at short times. This process is a Rouse process: the chain end fluctuates and needs a certain time $\tau_{\text{early}}(x)$ to cover a normalized distance d_x from its initial position and relax a fraction x of the tube, as described by Eq. (9). However, these relaxation times have been determined based on the assumption that the tube around the chain is a sequence of N/N_e segments, each being a random walk of N_e

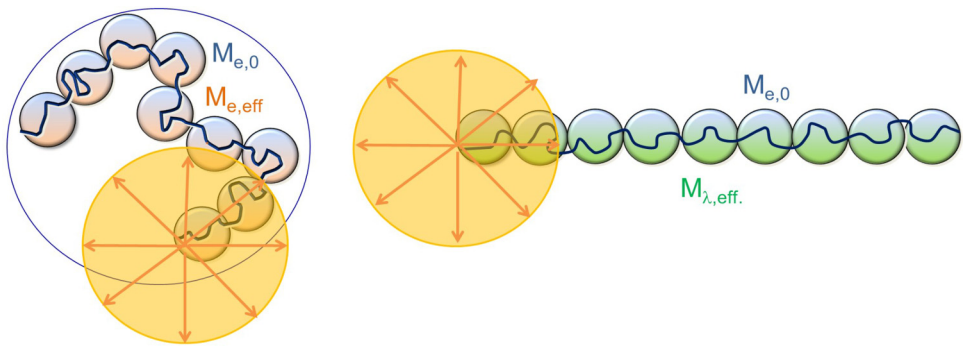

FIG. 9. Illustration of a polymer chain relaxing at the extremities by CLF, in the linear regime (left) or in the intermediate regime where chain blobs are oriented (right). In the latter regime, only fluctuations faster than $1/\dot{\varepsilon}$ can take place. Furthermore, at a given time, the area explored by the chain extremities through these fast fluctuations ($\tau_{\text{fluc}} < 1/\dot{\varepsilon}$) does not depend on tube orientation; however, the area of the curvilinear tube explored and thus the fraction of the initial tube, which is relaxed by these early fluctuations, is more important in the linear regime.

monomers, which is not valid anymore if the tube is oriented: while in the linear regime, the chain end of an unentangled linear chain needs to diffuse a distance $R = \sqrt{N}b$ in order to fully relax by a Rouse process (thus leading to a Rouse time $\tau_R \sim R^2/D$, where D is the diffusion coefficient), it has to diffuse a distance $L = Zl = Z\sqrt{N_e}b\ \lambda_{st}$ if the tube is fully oriented and possibly stretched as well. In the steady-state regime, we therefore expect a delay in the fluctuation time of the tube segments, equal to $L^2/R^2 = Z\lambda_{st}^2$ if the tube is fully oriented. At high stretch rates, this delay is large enough to justify the assumption that the chains cannot relax by CLF. However, at intermediate rates, the tube is only partially oriented and we can no longer neglect the CLF process, as it was proposed in Sec. IV B. Assuming that a fraction $\varphi_{\dot{\varepsilon}}$ of the tube is oriented, we therefore determine a delay factor in the CLF process, such that it ranges from 1 in the linear regime to $Z\lambda_{st}^2$ if the tube is fully oriented,

$$\tau_{fluc}^{\dot{\varepsilon}}(x) = \{\varphi_{\dot{\varepsilon}}\, Z\lambda_{st}^2 + (1-\varphi_{\dot{\varepsilon}})\}\ \tau_{fluc}(x). \tag{26}$$

In the above equation, the average tube orientation $\varphi_{\dot{\varepsilon}}$ is determined by considering that the flow can only orient the tube segments that are not relaxed in the steady-state regime [see Eq. (9)],

$$\varphi_{\dot{\varepsilon}} = \dot{\varepsilon}\int_0^\infty \varphi(t)dt = \dot{\varepsilon}\int_0^\infty \sum_x e^{\frac{-t}{\tau_x}}dxdt = \sum_x \dot{\varepsilon}\tau_x dx, \tag{27}$$

with $\varphi_{\dot{\varepsilon}} \leq 1$.

Therefore, in order to capture the transitional regime, Eq. (26) must be used instead of Eq. (9), to determine the relaxation time of a tube segment and, consequently, to determine the unrelaxed fraction of the initial tube segments, φ(t) [see Eq. (7)]. Thus, φ(t) is now a function of the deformation rate and includes the effect, on the relaxation time spectrum, of the average deformation state the chain is expected to reach given a certain flow rate.

b. Influence of the elongational flow strength on the CR process. The evolution of the number of effective blobs per entanglement segment (blob factor), $\Phi_{eff,\dot{\varepsilon}}(t)$, is defined as proposed in Eq. (22), i.e., accounting for (1) the entanglements, which constrain the motion of a test chain within a tube (φ), (2) the time necessary for a chain segment at equilibrium to explore its surroundings by a Rouse process [$5/4\sqrt{\tau_e/2t}$, see Eq. (13)], and (iii) the reduction of the size

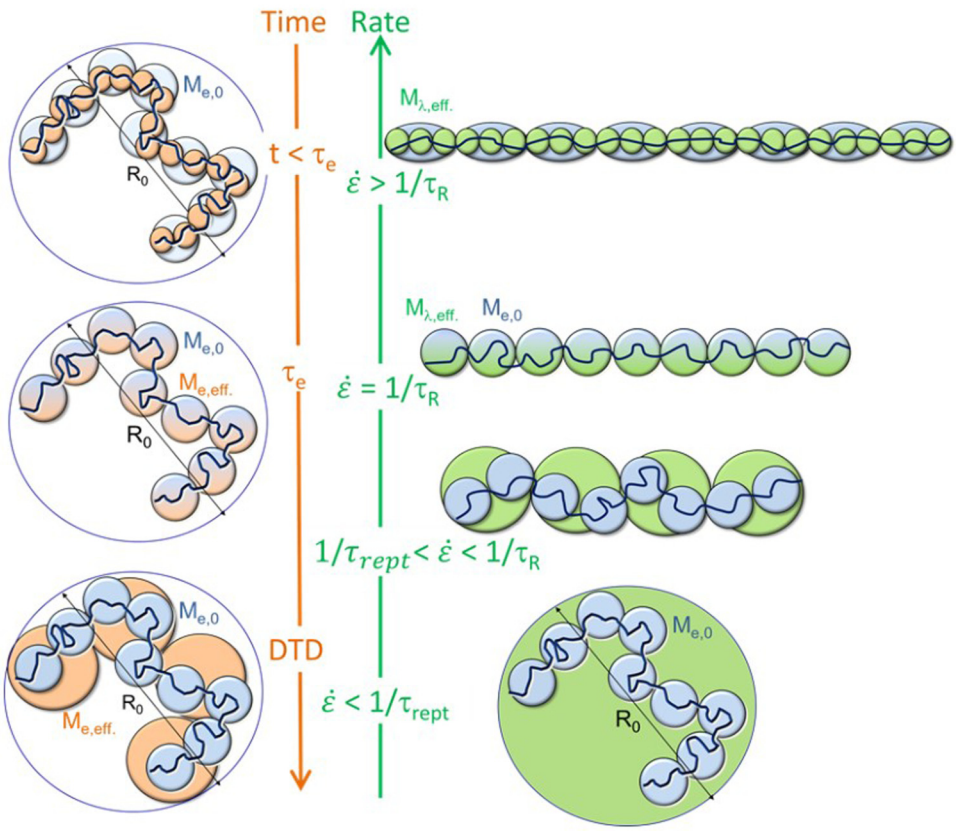

FIG. 10. Illustration of the blob picture representing the effective blob factor $\Phi_{eff,\dot{\varepsilon}}(t)$ evolving with time (on the left side) or with elongation rate (on the right side). $\Phi_{eff,\dot{\varepsilon}}(t)$ defines the molar mass $M_{e,0}/\Phi_{eff,\dot{\varepsilon}}(t)$ of the smallest subchains elastically active at time t and at an elongation rate $\dot{\varepsilon}$ [see Eq. (22)] and is equal to the number of Gaussian blobs per entanglement segment of mass $M_{e,0}$. In the linear regime, the mass of these subchains, $M_{e,eff}$ (t) (represented by the orange blobs), increases with the chain relaxation: at short times, it is first constrained by the size of the blobs that a chain can explore by Rouse process, $\Phi_{eff,\dot{\varepsilon}}(t) = (5/4)\sqrt{\tau_e/2t}$. Then, at time $t > \tau_e$, it is constrained by the entanglements and $\Phi_{eff,\ \dot{\varepsilon}}(t) = 1$. At longer times, the chains (partially) relax and can explore a larger tube through DTD, $\Phi_{eff,\dot{\varepsilon}}(t) = \varphi(t)$. In the nonlinear regime, the same picture holds; however, the flow-induced alignment or stretch imposes an additional limit on the size of the smallest subchains, which are internally but not mutually equilibrated, $\Phi_{eff,\dot{\varepsilon}}(t) > \Phi_{\lambda}(\dot{\varepsilon})$ or equivalently, $M_{e,eff} < M_{\lambda,eff}$ (with $M_{\lambda,eff} = M_{e,0}/p_{eq,ent}$), as represented by the green blobs. As soon as $M_{\lambda,eff}$ becomes smaller than $M_{e,eff}$ (t), transient strain hardening is observed.

of the internally equilibrated chain segments due to the stretch ($\Phi_\lambda(\dot{\varepsilon})$). As illustrated in Fig. 10, Eq. (22) considers that these three mechanisms are inter-related since they all define the molar mass $M_{e,\mathrm{eff}} = M_{e,0}/\Phi_{\mathrm{eff},\dot{\varepsilon}}$ of the largest chain segment, which is Gaussian. Therefore, they cannot be considered independently. While at rates smaller than $1/\tau_{\mathrm{rept}}$ the elongational flow has no effect on $M_{e,\mathrm{eff}}$, it does control $M_{e,\mathrm{eff}}$ at rates larger than $1/\tau_R$ (see Sec. IV B). At intermediate rates, since the (equilibrium) entanglement segments are not stretched ($\lambda \leq 1$), $\Phi_\lambda(\dot{\varepsilon})$ ($= 2\sqrt{\tau_{\lambda,\mathrm{ent}}\dot{\varepsilon}}$) never exceeds 1. However, as discussed in [63], it can still influence $\Phi_{\mathrm{eff},\dot{\varepsilon}}(t)$ if its value is larger than the dilution factor $\Phi = \varphi$, since in such a case the DTD process is limited to a tube diameter compatible with the one imposed by the flow, $a_\lambda = a_0\Phi_\lambda^{-1/2}$. In other words, it is possible that the diluted tube segments (of mass $M_{e,0}/\varphi$) stretch under flow, while the equilibrium tube segments (of mass $M_{e,0}$) do not. This flow-induced reduction of the effective tube diameter also leads to transient hardening, observed as soon as $\Phi_\lambda(\dot{\varepsilon})$ is becoming larger than $\varphi(t)$ [see Eq. (22)].

In addition to the limitation of the effective tube diameter, the stretch relaxation time of an entanglement segment $\tau_{\lambda,\mathrm{ent}}$ is expected to be shorter compared to a fully oriented tube [see Eq. (18)] in case the tubes are not fully oriented or stretched, which is the case in this intermediate regime ($1/\tau_d < \dot{\varepsilon} < 1/\tau_R$). In particular, in the limit of low elongational rates, this time should tend toward τ_R. We, therefore, approximate it as

$$\tau_{\lambda,\mathrm{ent}}(\dot{\varepsilon}) = \max(1,\ \varphi_{\dot{\varepsilon}}\ \theta)\ \tau_R. \tag{28}$$

In Fig. 11, predictions are obtained based on Eqs. (26) and (28) in the modified model and compared against experimental data. Using $\theta = 3.1$, a very good agreement is found for all molar masses examined. In particular, the viscosity upturn observed with low molar mass samples, PS100 and PS50, is well captured, which suggests that limiting the influence of CLF and CR processes in function of the orientation and stretch state of the chains leads to an alternative way to explain their elongational properties, without having to invoke any additional process.

In the case of the unentangled PS27, the chains are unentangled and only relax by a Rouse process. Therefore, accounting for the stretch of the chain, the corresponding relaxation modulus [Eq. (16)] is reformulated as

$$G(t) = G_N^0 \exp\left(\frac{-2t}{\tau_R}\right)\Phi_C(t)\max\left(\frac{5}{4}\sqrt{\frac{\tau_e}{2t}},\ 2\sqrt{\tau_{\lambda,\mathrm{ent}}\dot{\varepsilon}}\right). \tag{29}$$

Furthermore, the average chain orientation, $\varphi_{\dot{\varepsilon}}$, used to determine $\tau_{\lambda,\mathrm{ent}}$ should here only depend on the main Rouse time of the chain so that in this case Eq. (28) utilizes a modified $\varphi_{\dot{\varepsilon},R}$,

$$\varphi_{\dot{\varepsilon},R} = \frac{\tau_R}{2}\dot{\varepsilon}, \quad \text{with } \varphi_{\dot{\varepsilon},R} \leq 1. \tag{30}$$

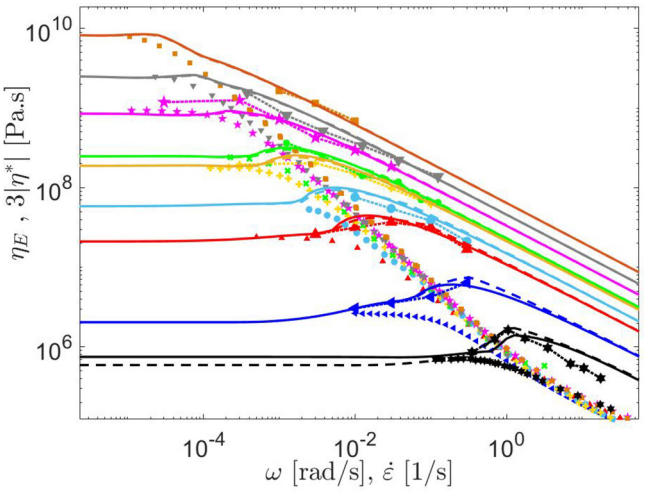

FIG. 11. Extensional viscosity versus elongational rate. Comparison between experimental data and predictions. Data are shown for PS545 (■), PS390 (▼), PS285 (*), PS200 (●), PS185 (+), PS133 (●), PS100 (▲), PS50 (◀), and PS27 (*) at $T - T_g = 23.4\,^{\circ}\mathrm{C}$. Apart from PS27, the continuous curves data are predicted by assuming polymer chains partially oriented in the intermediate regime of elongational rates [based on Eqs. (22)–(24), (26), and (28)]. For PS27, the continuous curve has been determined from Eqs. (29) and (30). The dashed curves have been predicted by considering that the chain extremities relax by a Rouse mechanism [see Eq. (31)].

The curve predicted for PS27 with Eq. (29) is also shown in Fig. 11, and a good agreement with the experimental data is found.

It should be noted that the two approaches used for determining the extensional viscosity of either entangled or unentangled chains can be combined into a single approach if we consider that the behavior of the last entanglement segment is governed by a Rouse relaxation, hence it does not depend on the tube [52]. This modification does not affect the relaxation of the long chains since their two end-segments represent a negligible fraction of the chain; however, it ensures that a polymer chain of molar mass lower than $2M_e$ fully relaxes by Rouse. In the model, this requires to consider the contribution from the chain extremities as separated term in the calculation of the average chain orientation, $\varphi_{\dot{\varepsilon}}$,

$$\varphi_{\dot{\varepsilon}} = \frac{2}{Z}\varphi_{\dot{\varepsilon},R} + \left(1 - \frac{2}{Z}\right)\max\left(\varphi_{\dot{\varepsilon},\mathrm{inner}},\ \varphi_{\dot{\varepsilon},R}\right), \tag{31}$$

with $\varphi_{\dot{\varepsilon},\mathrm{inner}}$ being the average orientation of the chain if the two outer segments are not accounted for

$$\begin{aligned}\varphi_{\dot{\varepsilon},\mathrm{inner}} &= \dot{\varepsilon}\int_0^\infty \varphi(t)dt \\ &= \dot{\varepsilon}\int_0^\infty \frac{\sum_{x_0}^{1} e^{\frac{-t}{\tau_{\dot{\varepsilon}}(x)}}dx}{1-x_0}dt = \frac{\sum_{x_0}^{1}\dot{\varepsilon}\tau_{\dot{\varepsilon}}(x)dx}{1-x_0}, \\ &\text{with } x_0 = \frac{1}{Z} \text{ and } \varphi_{\dot{\varepsilon},\mathrm{inner}} \leq 1,\end{aligned} \tag{32}$$

where $\varphi(t)$ represents the fraction of the original tube

segments that still exists at time t and $\tau_{\dot{\varepsilon}}(x)$ is the relaxation time of the tube segment x [see Eq. (26)].

This implies that only (Z-2) entanglement segments are oriented by $\varphi_{\dot{\varepsilon},\,\mathrm{inner}}$, while the two outer entanglement blobs are oriented by a free Rouse process, $\varphi_{\dot{\varepsilon},R}$.

Results found by using this combined approach are also shown in Fig. 11 as dashed curves. These predictions are only shown for the lower molar mass samples since no difference with the previous curves is observed for larger molar masses. A very good agreement between the experimental data and the model for both entangled and unentangled samples is obtained.

According to the microscopic picture proposed here, the elongational viscosity upturn observed for low molar mass samples (PS50 and PS100) can be seen as a transition between the linear regime of deformation and the regime where the chain is stretched at the scale of an entanglement segment. In fact, this result appears to be rather meaningful in retrospect if we simply consider the scaling of the steady viscosity with $\eta_E \sim M^{3.4}$ in the linear regime, while $\eta_E \sim M$ in the high strain rate regime (see Fig. 7) [46]. Therefore, a transition zone must exist between these two regimes if the direct intersect of the two scaling regimes appears at rates larger than the inverse Rouse time.

C. Nonlinear elongational properties in the transient regime

In order to describe the tensile stress growth coefficient, we start from the differential approximation of the McLeish and Larson model [58], which was initially derived for pom-pom polymers, and is the basis of a wide range of models describing the tensile stress growth coefficient data of polymer melts [21,26,38,80]. In this model, the polymeric stress tensor $\boldsymbol{\sigma}$ is defined by Eq. (2), and the orientation tensor $\boldsymbol{S}$ is obtained from the normalization of the deformation tensor $\boldsymbol{A}$, which accounts for both the flow-induced orientation of the entanglement segments and their possible relaxation,

$$\boldsymbol{S}(t) = \frac{\boldsymbol{A}(t)}{\mathrm{trace}(\boldsymbol{A}(t))}, \tag{33}$$

$$\frac{d\boldsymbol{A}}{dt} = \boldsymbol{\kappa}.\boldsymbol{A} + \boldsymbol{A}.^{T}\boldsymbol{\kappa} - \frac{1}{\tau_d}\left(\boldsymbol{A} - \frac{\boldsymbol{I}}{3}\right),\ \boldsymbol{A}(t=0) = \frac{\boldsymbol{I}}{3}, \tag{34}$$

where τ_d is the terminal relaxation time of the chain and $\boldsymbol{\kappa}$ is the velocity gradient tensor. In the case of an uniaxial extensional flow of a strain rate $\dot{\varepsilon}$, it is equal to

$$\boldsymbol{\kappa} = \begin{pmatrix} \dot{\varepsilon} & 0 & 0 \\ 0 & -\dot{\varepsilon}/2 & 0 \\ 0 & 0 & -\dot{\varepsilon}/2 \end{pmatrix}. \tag{35}$$

The stretch of an entanglement segment is given by the differential Eq. (17), while accounting for the average orientation of the entanglement segments,

$$\frac{d\lambda}{dt} = \lambda\boldsymbol{\kappa}.\boldsymbol{S} - \frac{\lambda - 1}{\tau_R}, \qquad \lambda(t=0) = 1. \tag{36}$$

It should be noted that according to this model, the stretch along the chain backbone is approximated to be constant, which is a rather strong assumption. A similar assumption was used in previous works for linear chains [21,32,34,36,38], while in the case of branched polymers, its value is usually considered constant along a specific branch or backbone but differs for each generation [26,27,58,80].

The tensile stress growth coefficient is finally obtained from the stress of Eq. (2) and the extensional flow field described by Eq. (35),

$$\eta_E^{+}(t) = \frac{3}{\dot{\varepsilon}} G_N^0 (S_{zz} - S_{rr})\lambda^2, \tag{37}$$

where S_{zz} and S_{rr} are the axial and the radial orientation component. In order to account for CLF and the reptation time of each segment x along the tube, we use here the modification proposed by Blackwell *et al.* [80], which considers an individual orientation tensor $\boldsymbol{S}(x,t)$ and deformation tensor $\boldsymbol{A}(x,t)$ for each segment x,

$$\boldsymbol{S}(x,\,t) = \frac{\boldsymbol{A}(x,\,t)}{\mathrm{trace}(\boldsymbol{A}(x,\,t))}, \tag{38}$$

$$\begin{aligned} \frac{d\boldsymbol{A}(x,\,t)}{dt} &= \boldsymbol{\kappa}.\boldsymbol{A}(x,\,t) + \boldsymbol{A}(x,\,t).^{T}\boldsymbol{\kappa} \\ &\quad - \frac{2}{\tau(x)}\left(\boldsymbol{A}(x,\,t) - \frac{\boldsymbol{I}}{3}\right), \\ \boldsymbol{A}(x,\,t=0) &= \frac{\boldsymbol{I}}{3}, \end{aligned} \tag{39}$$

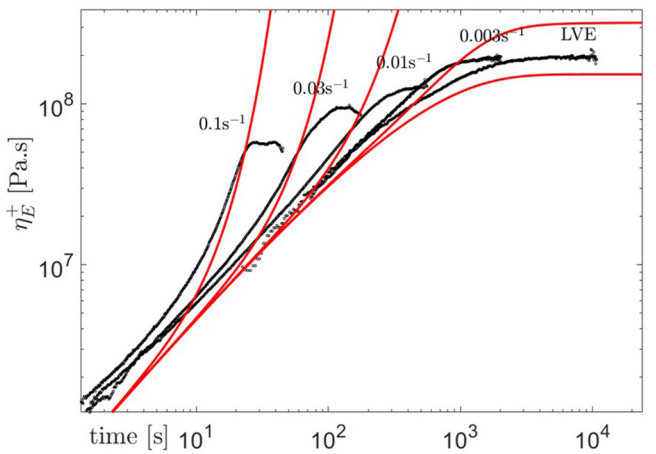

FIG. 12. Comparison between tensile stress growth coefficient data (symbols) of PS185 at $\dot{\varepsilon}$ indicated by the numbers, and the original McLeish and Larson model (red curves) without considering early Rouse relaxation. The data are taken from [16].

$$\boldsymbol{\sigma} = 3G_N^0\lambda^2 \int_{x=0}^{1} \boldsymbol{S}(x,t)\frac{d\varphi(x)\Phi(x)}{dx}dx, \tag{40}$$

where $\tau(x)$ is the relaxation time of the segment x in the linear regime of deformation [see Eq. (8)]. The factor 2 in Eq. (39) accounts for DTD, which effectively speeds up the chain relaxation. In Eq. (40), $\Phi(x)$ accounts for CR influence and $\varphi(x)$ is equal to the fraction of initial tube segments which have not yet relaxed when the segment x is relaxing. For a monodisperse linear sample, this function can be approximated by $\varphi(x) = \Phi(x) = 1 - x$, considering all segments before x are already relaxed when x is relaxing. In Eq. (40), the stretch of an entanglement segment, $\lambda(t)$, is also considered constant along the chain backbone, being a function of the average orientation of the primitive path [see Eq. (36)].

In Fig. 12, Eqs. (36)–(40) are tested on a representative sample, PS185. In addition to the unsatisfactory agreement

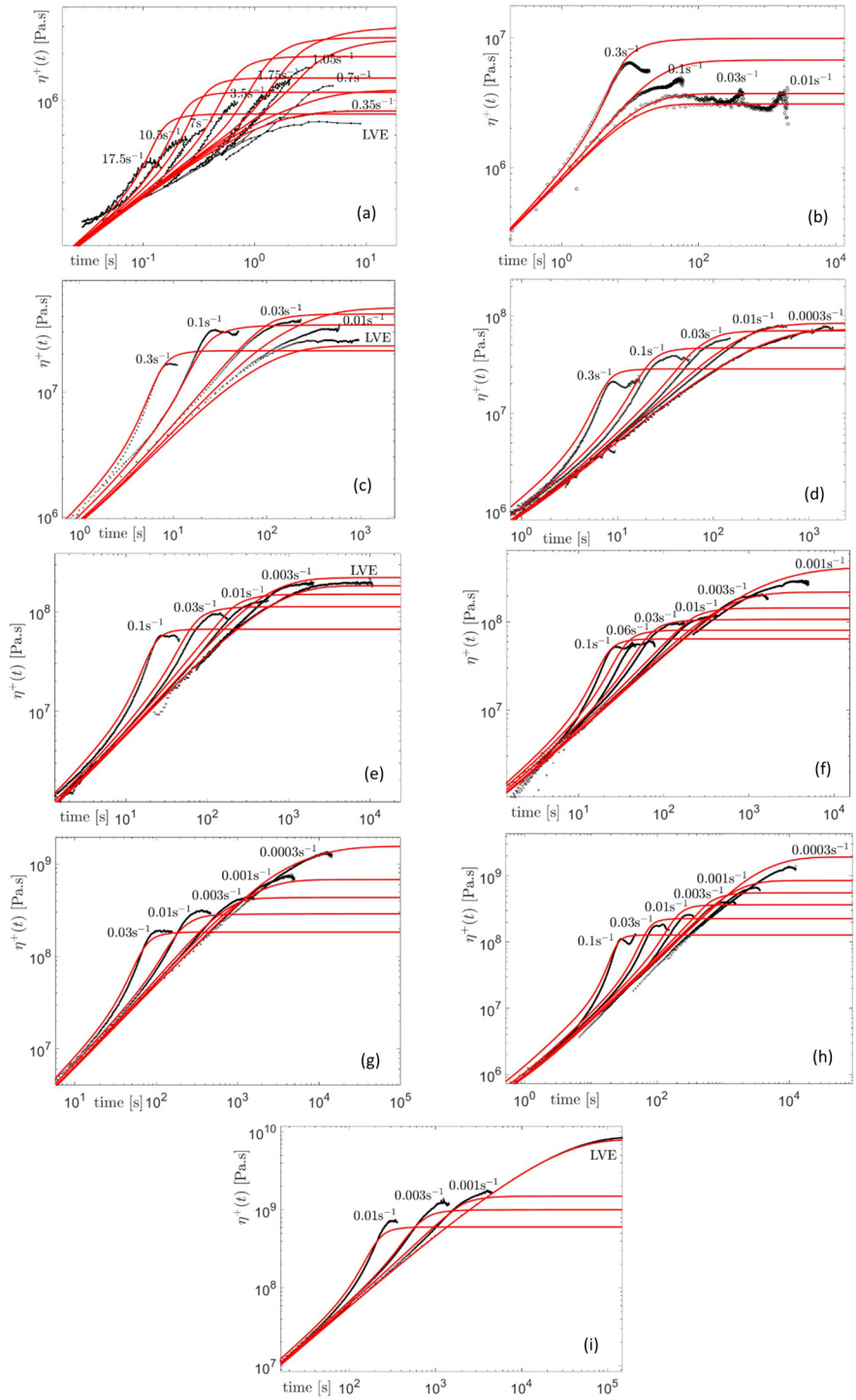

FIG. 13. Tensile stress growth coefficient as a function of time for monodisperse melts. Comparison between experimental data and predictions of the modified McLeish and Larson model. Data are shown for (a) PS27, (b) PS50, (c) PS100, (d) PS133, (e) PS185, (f) PS200, (g) PS285, (h) PS390, and (i) PS545 at different extension rates indicated by the numbers, for $T - T_g = 23.4$ °C.

found for predicting the linear envelop, the stretch evolution shows an unbounded increase, as discussed in Sec. IV A. In order to limit the stretch, a finite extensibility criterion should be added. However, as discussed in Sec. I, finite extensibility is not reached in this case.

We, therefore, modify these equations according to the discussions in Secs. III and IV: first to correct the LVE envelop, and then to include the contribution of all Rouse modes to stretch relaxation. First, since the early Rouse relaxation is not accounted for in the original model, we use a similar approach as in Sec. III A to include its effect, considering $\Phi_{\text{eff}}(x)$ [see Eq. (13)] in place of the dilution factor $\Phi(x)$ in Eq. (40): for $\dot{\varepsilon} < 1/\tau_R$,

$$\Phi_{\text{eff}}(x) = \min\left(N_e,\ \max\left(\varphi(x),\ \sqrt{\frac{\tau_e}{2\tau(x)}}\right)\right), \tag{41}$$

where N_e ensures that the fastest Rouse mode is the mode N that corresponds to the relaxation of a Kuhn segment. Furthermore, $\varphi(x)$ also needs to be modified in order to account for the fact that the tube does not exist up to $x_0 = 1/Z$. Therefore, $\varphi(x)$ in Eq. (40) needs to be rescaled as

$$\varphi(x) = \min\left(1,\ \frac{1-x}{1-x_0}\right). \tag{42}$$

Using Eqs. (41) and (42) in Eq. (40) allows to accurately describe the LVE properties of the samples (see Fig. 13).

In order to account for the possible stretch of the entanglement segments, we consider the influence of all the Rouse modes to describe the evolution of the stretch (Sec. IV A). To this end, Eq. (19) is used, but including now the evolution of the tube orientation $\varphi_{\dot{\varepsilon},t}$ with time (in the steady regime, at high elongation rates, $\varphi_{\dot{\varepsilon},t} = 1$),

$$\frac{d\lambda}{dt} = \lambda\dot{\varepsilon}\varphi_{\dot{\varepsilon},t} - \frac{\lambda - \sqrt{\lfloor\lambda^2\rfloor}}{\tau_{\lambda,\text{ent}}/\lfloor\lambda^2\rfloor^2} - \sum_{p=1}^{\lfloor\lambda^2\rfloor-1}\frac{\sqrt{p+1}-\sqrt{p}}{\tau_{\lambda,\text{ent}}/p^2}, \tag{43}$$

where the tube orientation $\varphi_{\dot{\varepsilon},t}$ is expressed in a similar way as in Eq. (31),

$$\varphi_{\dot{\varepsilon},t} = \frac{2}{Z}S_R(t) + \left(1-\frac{2}{Z}\right) \times \max\left(\int_{x=x_0}^{1}(S_{zz}(x,t) - S_{rr}(x,t))\frac{dx}{1-x_0},\ S_R(t)\right). \tag{44}$$

In this equation, $S_R(t) = (S_{R,zz}(t) - S_{R,rr}(t))$ corresponds to the orientation of a chain segment at time t relaxing at time $\tau_R/2$ and calculated using Eqs. (38) and (39).

Furthermore, the CR mechanisms induced by tube dilution are limited by the tube stretch, which limits the increase in the tube diameter or equivalently limits the decrease in $\Phi_{\text{eff}}(x)$. As these two terms are linked, Eqs. (40) and (41) are modified to account for both the limitation of CR mechanisms and tube stretch within a single term, the effective blob factor,

$$\Phi_{\text{eff},\dot{\varepsilon}}(x) = \min\left(N_e,\ \max\left(\lambda^2\max\left(\varphi(x),\ \varphi_{(\dot{\varepsilon}),t},\ \sqrt{\frac{\tau_e}{2\tau(x)}}\right)\right)\right). \tag{45}$$

Thus,

$$\boldsymbol{\sigma} = 3G_N^0\int_{x=0}^{1}\boldsymbol{S}(x,t)\frac{d\varphi(x)\Phi_{\text{eff},\dot{\varepsilon}}(x)}{dx}dx. \tag{46}$$

Finally, to take into account CLF hindrance, $\tau(x)$ in Eq. (39) is replaced by $\tau_{\dot{\varepsilon}}(x)$ calculated from Eq. (26), while considering $\varphi_{\dot{\varepsilon},t}$.

The results obtained with this new set of Eqs. (26), (37)–(39), and (42)–(46) are compared to experimental data in Fig. 13. There is a relatively good agreement over a wide range of molar masses, and, more importantly, with the steady-state model (see Fig. 16). As detailed in Appendix C, the similarity between the TMA and the modified ML models is not surprising since both account for the different relaxation processes and for the influence of the chain stretch in a similar way. Their main difference is the fact that the TMA model describes the dilution factor as a function of time, $\Phi(t)$, while in the modified ML model, it must be expressed as a function of the tube segment x, $\Phi(x)$. However, as long as the same coarse-grained microscopic picture is used, the results should not be model-dependent, as it is shown in Fig. 15. Basically, x and t are related since the chain relaxation of a specific segment x takes place at a specific time t.

It must also be noted that the modified ML model does not directly apply to the prediction of the tensile stress growth coefficient of the unentangled sample PS27 and, as expected, a larger discrepancy is obtained for this sample, in particular, when describing its LVE envelop.

V. CONCLUSIONS

In this work, we have addressed the elongational viscosity of linear entangled polymers and, in particular, we have presented an analysis framework which is an alternative to the current one. We have presented two approaches. First, we have proposed a simple approach, based on the extended use of the blob picture of Pincus, to predict the nonlinear extensional steady-state viscosity of monodisperse PS melts without considering any additional mechanism or criterion to explain the different scaling observed experimentally. There is, however, one parameter, θ, which controls the stretch relaxation time of chain entanglements and needs to be adjusted. This parameter should not depend on the composition of the polymer melts, as it has been observed experimentally and based on simulations, as discussed in Sec. I. However, it most probably depends on the sample chemistry and chain flexibility [46,48,60]. This first approach starts from the idea that the evolution of the chain stretch depends on the different Rouse relaxation modes [56,57] and considers that the modes with a relaxation time shorter than the inverse extensional rate do not contribute to the stretch. Consequently, at strain rates larger

than $1/\tau_R$ but shorter than the inverse relaxation time of a Kuhn segment, $1/\tau_0$, the chains stretch saturates in the steady regime at a value below the finite extensibility limit, in agreement with the experimental observations discussed in Sec. I. Furthermore, it was considered that the flow-induced chain stretching limits the chain motions in the lateral direction to the primitive path, which leads to an increase in the number of internally but not mutually equilibrated blobs within an entanglement segment and to a reduced influence of CLF and DTD processes. By accounting for this gradual suppression of CLF and CR processes with increasing the elongation rate, we therefore ensure that the relaxation state of the chains is compatible with the flow-induced orientation of the entanglement segments and, at higher strain rate, with their stretch. In particular, this allows to define an effective tube diameter, $a_\lambda = a_0 \Phi_{\text{eff},\dot{\varepsilon}}^{-1/2}$, which represents the tube diameter that an entanglement segment has time to explore, and which includes, in addition to the CR process, the limitations imposed by local Rouse relaxation of the chains at short times as well as by the chain stretch at high rates.

Compared to the friction reduction model, our approach starts from another—yet not necessarily incompatible—point of view. Indeed, the friction reduction model is based on the assumption that for elongational rates above the inverse Rouse time, the chains should reach their finite extensibility; however, the FENE effect competes with the friction reduction, which limits the steady viscosity. Thus, the higher the strain rate, the more important the friction reduction is, and the more the steady viscosity reduction is, compared to the steady viscosity predicted by the FENE limit. On the other hand, our approach starts from the assumption that the FENE limit is not reached because of the existence of the fast equilibration modes, which enable a partial equilibration of the chains and therefore limit their final stretch. Here, the larger strain rate leads to a larger number of internally equilibrated blobs in an entanglement segment; larger stretch and larger value of the steady-state viscosity compared to its value determined without accounting for chain stretch (which scales with $\dot{\varepsilon}^{-1}$). Because of these different starting points, the comparison between the two approaches is not straightforward and goes beyond the scope of this work. For example, larger differences may appear in the viscoelastic responses of binary blends of linear chains, since according to our approach, the steady stretch of a chain should not depend on its environment, while according to the friction reduction model, it does.

In a second approach, we modified the nonlinear pom-pom model of McLeish and Larson in order to predict the transient extensional response of the linear polymers, while keeping the same microscopic picture proposed in the first approach. The similarity between the results obtained, which is discussed in Appendix C, allows us to conclude that the modifications proposed in the present paper to describe the steady-state stretch and the influence of the latter on the relaxation processes are general and similar results could have been obtained with an equivalent modification of any other tube model.

The satisfactory agreement found with the experimental data is encouraging. In a recent work, we show that the same blob picture can also be used to describe the response of linear chains under shear flow [75]. As prospective future research, we shall investigate the elongation behavior of entangled polymer solutions in order to explore if and how the viscosity upturn can also in this case be seen as a transition zone between the linear regime and the large strain rate regime in which the chains are stretched. In a recent experimental study on the elongational properties of polymer blends and solutions [81], it was shown that for bidisperse blends with both components stretched, a linear scaling law can be used to describe the elongational viscosity; however, this scaling does not hold if one of the components is too short to be stretched, in agreement with the results of [15,29]. More precisely, it was shown in [81] that the tensile stress growth coefficient of a chain does not depend on sample composition, but its steady-state value does in case the blend contains a short component. Therefore, the model proposed here is expected to correctly describe the steady-state elongational viscosity of polymer melts but not that of solutions, as the solvent cannot stretch/orient. This will be further explored in future work.

ACKNOWLEDGMENTS

The authors thank Hiroshi Watanabe, Ole Hassager, Qian Huang, Michael Rubinstein, Shura Grosberg, Salvatore Costanzo, and Laurence Hawke for very helpful discussions and for sharing experimental data. The anonymous reviewers are also acknowledged for their valuable comments. This work was funded by DSM Materials Science Center (for T.S. and C.H.), the Bijzonder Onderzoeksfonds KU Leuven (GOA 15/007) for C.C., and the F.N.R.S. [for C.H. (FRIA) and E.V.R. as Senior Research Associate].

APPENDIX A: DERIVATION OF EQ. (19).

At equilibrium, the length of the primitive path of a linear chain is $L_{\text{eq}} = \sqrt{ZNb^2}$, which corresponds to a stretch factor $\lambda = L/L_{\text{eq}} = 1$.

In order to determine the stretch factor in the nonlinear regime of deformation, we consider that the Rouse mode p allows the relaxation of a stretched chain down to a length $L_p = \sqrt{pZNb^2}$, within a time $\tau_{\lambda,p} = \tau_{\lambda,\text{ent}}/p^2 = \theta\tau_R(M)/p^2$, where $\tau_{\lambda,\text{ent}}$ is the stretch relaxation time of a stretched tube segment.

However, considering that the chain always relaxes according to the faster possible mode, the Rouse mode p with time $\tau_{\lambda,p}$ will be effective in relaxing a stretched chain segments with length between $L_{p+1} = \sqrt{(p+1)ZNb^2}$ and $L_p = \sqrt{pZNb^2}$. Therefore, the contribution of each mode p to the relaxation of a stretched tube can be written as $[(L_{p+1} - L_p)/\sqrt{(ZNb^2)}]*1/\tau_{\lambda,p} = (\sqrt{(p+1)} - \sqrt{(p)})/\tau_{\lambda,p}$, where $(L_{p+1} - L_p)/\sqrt{ZNb^2}$ is the fraction of the stretch relaxed between $\tau_{\lambda,p+1}$ and $\tau_{\lambda,p}$.

Summing up the contribution from each mode, starting from mode $p = 1$ up to mode $p = \lambda^2$ (since the length of the stretched tube is $L = \lambda L_{\text{eq}} = \sqrt{\lambda^2 ZNb^2}$) leads to a differential equation describing the stretch relaxation of a fully oriented

tube,

$$\frac{dL}{dt} = L\dot{\varepsilon} - \frac{L - \sqrt{\lfloor\lambda^2\rfloor ZNb^2}}{\tau_{\lambda,\lfloor\lambda^2\rfloor}} - \sum_{p=1}^{\lfloor\lambda^2\rfloor-1} \frac{\sqrt{(p+1)ZNb^2} - \sqrt{pZNb^2}}{\tau_{\lambda,p}}, \quad \text{(A1)}$$

or equivalently,

$$\frac{d\lambda\sqrt{ZNb^2}}{dt} = \lambda\sqrt{ZNb^2}\dot{\varepsilon} - \frac{\lambda\sqrt{ZNb^2} - \sqrt{\lfloor\lambda^2\rfloor ZNb^2}}{\tau_{\lambda,\lfloor\lambda^2\rfloor}} - \sum_{p=1}^{\lfloor\lambda^2\rfloor-1} \frac{\sqrt{(p+1)ZNb^2} - \sqrt{pZNb^2}}{\tau_{\lambda,p}}, \quad \text{(A2)}$$

i.e.,

$$\frac{d\lambda}{dt} = \lambda\dot{\varepsilon} - \frac{\lambda - \sqrt{\lfloor\lambda^2\rfloor}}{\tau_{\lambda,\lfloor\lambda^2\rfloor}} - \sum_{p=1}^{\lfloor\lambda^2\rfloor-1} \frac{\sqrt{p+1} - \sqrt{p}}{\tau_{\lambda,p}} = \lambda\dot{\varepsilon} - \frac{\lambda - \sqrt{\lfloor\lambda^2\rfloor}}{\tau_{\lambda,\text{ent}}/\lfloor\lambda^2\rfloor^2} - \sum_{p=1}^{\lfloor\lambda^2\rfloor-1} \frac{\sqrt{p+1} - \sqrt{p}}{\tau_{\lambda,\text{ent}}/p^2}. \quad \text{(A3)}$$

Hence,

$$\frac{d\lambda}{dt} = \lambda\dot{\varepsilon} - \frac{\lambda - \sqrt{\lfloor\lambda^2\rfloor}}{\tau_{\lambda,ent}/\lfloor\lambda^2\rfloor^2} - \sum_{p=1}^{\lfloor\lambda^2\rfloor-1} \frac{\sqrt{p+1} - \sqrt{p}}{\tau_{\lambda,ent}/p^2}. \quad \text{(A4)}$$

When $\lambda^2 < 2$, the upper limit of the sum, $\lfloor\lambda^2\rfloor - 1$, is equal to zero. In this specific case, this term has to be disregarded and Eq. (19) reduces to $d\lambda/dt = \lambda\dot{\varepsilon} - (\lambda - 1)/\tau_{\lambda,\text{ent}}$.

APPENDIX B: DERIVATION OF Eq. (20)

In the steady regime, Eq. (19) converges and we have

$$\frac{d\lambda}{dt} = 0 = \lambda_{\text{st}}(\dot{\varepsilon})\dot{\varepsilon} - \frac{\lambda_{\text{st}}(\dot{\varepsilon}) - \sqrt{\lfloor\lambda_{\text{st}}(\dot{\varepsilon})^2\rfloor}}{\tau_{\lambda,\text{ent}}/\lfloor\lambda_{\text{st}}(\dot{\varepsilon})^2\rfloor^2} - \sum_{p=1}^{\lfloor\lambda_{\text{st}}(\dot{\varepsilon})^2\rfloor-1} \frac{\sqrt{p+1} - \sqrt{p}}{\tau_{\lambda,\text{ent}}/p^2}, \quad \text{(B1)}$$

where $\lambda_{\text{st}}(\dot{\varepsilon})$ is the stretch reached in the steady regime.

In order to solve this equation, we first approximate $\sum_{p=1}^{\lfloor\lambda^2\rfloor-1}((\sqrt{p+1} - \sqrt{p})/(\tau_{\lambda,\text{ent}}/p^2))$ as $\sum_{p=1}^{\lfloor\lambda^2\rfloor-1} p^{3/2}/(2\tau_{\lambda,\text{ent}})$ [because $d\sqrt{x} = dx/(2\sqrt{(x)})$, and since $dx = 1$, we have $\sqrt{p+1} - \sqrt{p} \approx \sqrt{(p)}/2$].

We can approximate the latter expression as $[(\lambda^2 - 1)^{5/2} - 1]/(5\tau_{\lambda,\text{ent}})$ [since $\int_{x=1}^{\lfloor\lambda^2\rfloor-1} x^{3/2}/(2\tau_{\lambda,\text{ent}})dx = \left[(\lfloor\lambda^2\rfloor - 1)^{5/2} - 1\right]/(5\tau_{\lambda,\text{ent}})$ to finally obtain

$$\lambda_{\text{st}}(\dot{\varepsilon})\dot{\varepsilon} = \frac{\lambda_{\text{st}}(\dot{\varepsilon}) - \sqrt{\lfloor\lambda_{\text{st}}(\dot{\varepsilon})^2\rfloor}}{\tau_{\lambda,\text{ent}}/\lfloor\lambda_{\text{st}}(\dot{\varepsilon})^2\rfloor^2} + \frac{1}{5\tau_{\lambda,\text{ent}}}[(\lfloor\lambda_{\text{st}}(\dot{\varepsilon})^2\rfloor - 1)^{5/2} - 1]. \quad \text{(B2)}$$

For a stretched chain with $\lfloor\lambda^2\rfloor \gg 1$, this expression is equivalent to $\lambda_{\text{st}}(\dot{\varepsilon})\dot{\varepsilon} = \lambda_{\text{st}}(\dot{\varepsilon})^5/(5\tau_{\lambda,\text{ent}})$ and therefore $\lambda_{\text{st}}(\dot{\varepsilon})^2 \approx \sqrt{5\tau_{\lambda,\text{ent}}\dot{\varepsilon}}$ [Eq. (20)].

APPENDIX C: COMPARISON OF THE TMA AND THE MODIFIED MCLEISH AND LARSON MODELS

We first compare the tube model (TMA) and the modified McLeish and Larson model (ML model) in the linear regime of deformation. Based on Eqs. (13) and (14), the simplified version of the TMA expresses the tensile stress growth coefficient in the linear regime of deformation as

$$\eta^+_{E,t}(t) = 3G^0_N \int_0^t [\varphi(t')\Phi_{\text{eff}}(t')]dt' = 3G^0_N \int_0^t \left[\int_x e^{-\frac{t'}{\tau(x)}}dx * \max\left(\int_x e^{-\frac{t'}{\tau(x)}}dx,\ \frac{5}{4}\sqrt{\frac{\tau_e}{2t'}}\right)\right]dt'. \quad \text{(C1)}$$

In this expression, the unrelaxed fraction of initial tube segments $\varphi(t)$ and the dilution factor $\Phi_{\text{eff}}(t)$ are expressed as functions of time and the viscosity is calculated as an integral over time of the unrelaxed fraction of initial tube segments. Alternatively, it is possible to express the tensile stress growth coefficient in the linear regime of deformation as a pondered sum over x of the average orientation of each segment x at time t,

$$\eta^+_{E,x}(t) = \frac{1}{\dot{\varepsilon}} 3G^0_N \int_0^x \mu(x,t)d[\varphi(x)\Phi_{\text{eff}}(x)], \quad \text{(C2)}$$

where $\mu(x, t)$ is the average orientation of the segment x induced by the flow at time t,

$$\mu(x,t) = \dot{\varepsilon}\int_0^t e^{-\frac{2t'}{\tau(x)}}dt'. \quad \text{(C3)}$$

In such a case, the unrelaxed fraction of initial tube segments φ and the dilution factor Φ_{eff} must also be expressed as functions of x. They correspond to $\varphi(t)$ and $\Phi_{\text{eff}}(t)$ at the time $t = \tau(x)/2$, at which the segment x is relaxing [note that $\tau(x)$ is divided by 2 to account for the effect of tube dilution]. Thus, $\varphi(x) = \varphi(t = \tau(x)/2)$ and $\Phi_{\text{eff}}(x) = \Phi_{\text{eff}}(t = \tau(x)/2)$.

These latter expressions can be simplified, based on the assumption that when the segment x is relaxing, all segments before x are already relaxed, leading to $\varphi(x) = 1 - x$ and $\Phi_{\text{eff}}(x) = \max\left(1 - x, (5/4)\sqrt{\tau_e/\tau(x)}\right)$. By combining these

expressions with Eqs. (C2) and (C3), we obtain

$$\eta^{+}_{E,x}(t) = 3G^0_N \int_0^x \int_0^t e^{-\frac{2t'}{\tau(x)}} dt' d\left[(1-x)\max\left(1-x, \frac{5}{4}\sqrt{\frac{\tau_e}{\tau(x)}}\right)\right]. \tag{C4}$$

Equations (C1) and (C4) are first compared in the linear regime of deformation. To this end, the corresponding relaxation moduli are calculated from the derivative of $\eta^{+}_{E,t}(t)$ and $\eta^{+}_{E,x}(t)$, as $G(t) = d\eta^{+}_{E}/dt$, and the respective complex moduli are determined from $G(t)$ by using the Schwarzl approximations [69]. The results obtained with both approaches are compared in Fig. (14). It is observed that both Eqs. (C1) and (C4) lead to similar results. Nevertheless, using Eq. (C4) leads to a slight and systematic underestimation of the final relaxation time of the chain, due to the fact that the tube dilution effect is taken into account by dividing $\tau(x)$ by 2, which does not account for the extra-term coming from $\varphi(t)\Phi_{\text{eff}}(t) \approx \varphi(t)^2 = \sum_x \left(\sum_y (exp^{(-t/\tau(x))} * exp^{(-t/\tau(y))})\right) dy * dx > \sum_x e^{-(2t/\tau(x))} dx$.

In the modified ML model, the tensile stress growth coefficient is expressed by Eq. (C2); however, the expression $\mu(x, t)$ is replaced by the subtraction of the zz and rr components of the individual orientation tensor $\boldsymbol{S}$, calculated by the differential equation [see Eq. (39)]. In Fig. 15, the results obtained based on Eqs. (38)–(42) with $\lambda = 1$ and considering a very slow rate of deformation are compared to the complex modulus obtained from the TMA. It is observed that the final relaxation time of both models is nearly identical; however, the plateau level is increasingly higher with the ML approach for smaller molar masses. This is due to the chain end correction applied in Eq. (42), $\varphi(x) = \min(1, (1-x)/1-x_0)$ instead of $\varphi(x) = 1-x$. To obtain similar results with the TMA, $\varphi(t)$ should also be rescaled starting from x_0: $\varphi(t) = (\int_{x_0}^{1} e^{-(t'/\tau(x))} dx/1 - x_0)$.

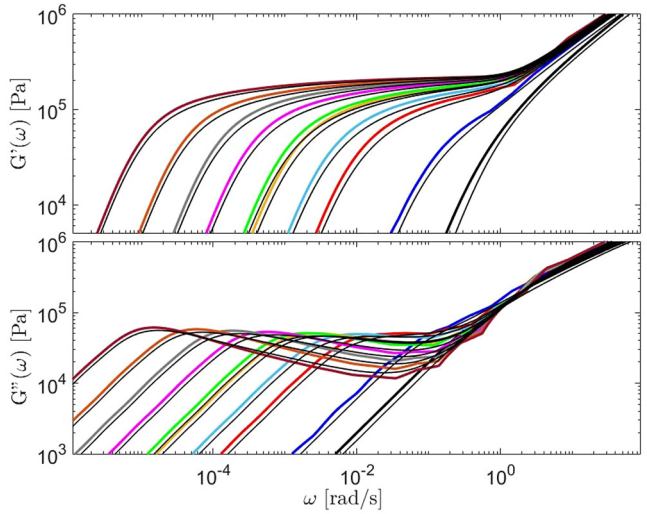

FIG. 14. Comparison between storage and loss moduli obtained from Eqs. C1 (thick colored curves) and C4 (thin black curves) for various PS molar masses (from left to right: PS820, PS545, PS390, PS285, PS200, PS185, PS133, PS100, PS50, and PS27).

This can be easily demonstrated: in the case of an unstretched chain, the ML model predicts

$$\begin{aligned}\eta_E(\dot{\varepsilon}) &= \lim_{t\to\infty}(3G^0_N/\dot{\varepsilon})\int_{x=0}^{1}(S_{zz}(x,t) - S_{rr}(x,t)) \\ &\times [(d\varphi(x)\Phi(x)/(dx))]dx \\ &\approx \frac{3G^0_N}{\dot{\varepsilon}}\int_{x=0}^{1} 2\left[\lim_{t\to\infty} S_{zz}(x,t) - S_{rr}(x,t)\right](1-x)dx,\end{aligned} \tag{C5}$$

with

$$\begin{aligned}\lim_{t\to\infty} S_{zz}(x,t) &= \frac{\lim_{t\to\infty} A_{zz}(x,t)}{\text{trace}\left(\lim_{t\to\infty}\boldsymbol{A}(x,t)\right)} \\ &= \frac{1}{3}\frac{\frac{2}{\tau_x} + 2\dot{\varepsilon}}{\frac{2}{\tau_x}} = \frac{1+\tau_x\dot{\varepsilon}}{3},\end{aligned} \tag{C6}$$

$$\begin{aligned}\lim_{t\to\infty} S_{rr}(x,t) &= \frac{\lim_{t\to\infty} A_{rr}(x,t)}{trace\left(\lim_{t\to\infty}\boldsymbol{A}(x,t)\right)} \\ &= \frac{1}{3}\frac{\frac{2}{\tau_x} - \dot{\varepsilon}}{\frac{2}{\tau_x}} = \frac{1-\frac{\tau_x\dot{\varepsilon}}{2}}{3},\end{aligned} \tag{C7}$$

$$\lim_{t\to\infty} S_{zz}(x,t) - S_{rr}(x,t) = \frac{\tau_x\dot{\varepsilon}}{2}. \tag{C8}$$

Therefore, the ML model predicts the extensional viscosity to be

$$\eta_E(\dot{\varepsilon}) \approx \frac{3G^0_N}{\dot{\varepsilon}}\int_{x=0}^{1}\tau_x\dot{\varepsilon}\,(1-x)dx. \tag{C9}$$

Equivalently, in this case, the TMA predicts the extensional viscosity in Eq. (23) to be

$$\begin{aligned}\eta_E(\dot{\varepsilon}) &= \int_0^\infty 3\,G^0_N\,\varphi(t)\Phi_C(t)\,\Phi_{eff,\dot{\varepsilon}}(t)\,dt \\ &\sim \int_0^\infty 3\,G^0_N\,\varphi(t)e^{-t\dot{\varepsilon}}\varphi(t)dt \\ &= \frac{3}{\dot{\varepsilon}}G^0_N\sum_x\sum_y \frac{\dot{\varepsilon}\tau_x}{1+\frac{\tau_x}{\tau_y}+\tau_x\dot{\varepsilon}}dxdy.\end{aligned} \tag{C10}$$

This sum can be rewritten as

$$\sum_x \sum_y \frac{\dot\varepsilon\tau_x}{1+\frac{\tau_x}{\tau_y}+\tau_x\dot\varepsilon}dxdy$$
$$=\sum_x \frac{\dot\varepsilon\tau_x}{2+\tau_x\dot\varepsilon}(dx)^2+2\sum_x\sum_{y>x}\frac{\dot\varepsilon\tau_x}{1+\frac{\tau_x}{\tau_y}+\tau_x\dot\varepsilon}dxdy$$
$$\in\left[2\sum_x\sum_{y\geq x}\frac{\dot\varepsilon\tau_x}{2+\tau_x\dot\varepsilon}dxdy,\,2\sum_x\sum_{y\geq x}\frac{\dot\varepsilon\tau_x}{1+\tau_x\dot\varepsilon}dxdy\right]$$
$$=\left[2\sum_x\frac{\dot\varepsilon\tau_x}{2+\tau_x\dot\varepsilon}(1-x)dx,\,2\sum_x\frac{\dot\varepsilon\tau_x}{1+\tau_x\dot\varepsilon}(1-x)dx\right]. \quad \text{(C11)}$$

Therefore, the TMA estimates the extensional viscosity to be

$$\frac{3}{\dot\varepsilon}G_N^0{}^*2\sum_x\frac{\dot\varepsilon\tau_x}{2+\tau_x\dot\varepsilon}(1-x)dx\leq\eta_E(\dot\varepsilon)\leq\frac{3}{\dot\varepsilon}G_N^0{}^*2\sum_x\frac{\dot\varepsilon\tau_x}{1+\tau_x\dot\varepsilon}(1-x)dx. \quad \text{(C12)}$$

In the limit of linear deformation ($\eta_E(\dot\varepsilon\to 0)$), Eq. (C9) leads to $\eta_E(\dot\varepsilon\to 0)=(3G_N^0/\dot\varepsilon)\int_{x=0}^1\tau_x\dot\varepsilon\,(1-x)dx$ and Eq. (C12) to $(3G_N^0/\dot\varepsilon)\int_{x=0}^1\tau_x\dot\varepsilon\,(1-x)dx \leq \eta_E(\dot\varepsilon\to 0)\leq 2[(3G_N^0)/(\dot\varepsilon)]\int_{x=0}^1\tau_x\dot\varepsilon\,(1-x)dx$, which confirms the similar results obtained in Fig. 15. However, for intermediate rates, these Eqs. (C9) and (C12) differ slightly, $2\sum_x[(\dot\varepsilon\tau_x)/(2+\tau_x\dot\varepsilon)](1-x)dx\leq\sum_x\tau_x\dot\varepsilon\,(1-x)dx \leq 2\sum_x[(\dot\varepsilon\tau_x)/(1+\tau_x\dot\varepsilon)](1-x)dx$, leading to a different predicted extensional viscosity as confirmed in Fig. 16 at intermediate rates.

The same considerations apply in the nonlinear regime of deformation: for a stretched chain, the ML model predicts

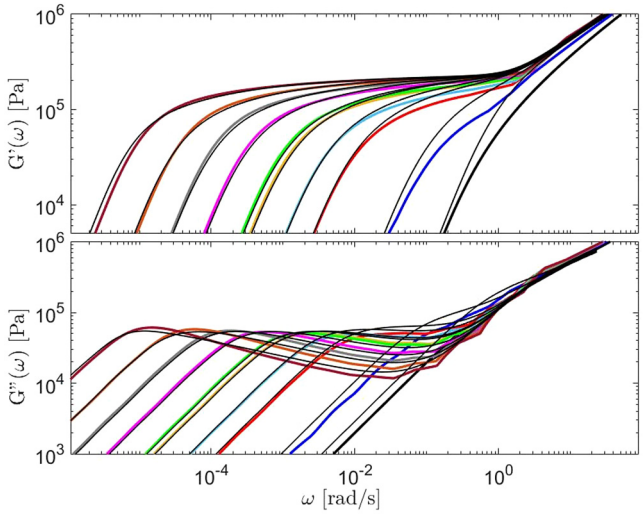

FIG. 15. Comparison between storage and loss moduli obtained from Eq. (C1) (thick colored curves) and the modified ML model (thin black curves) for various PS molar masses (from left to right: PS820, PS545, PS390, PS285, PS200, PS185, PS133, PS100, PS50, and PS27).

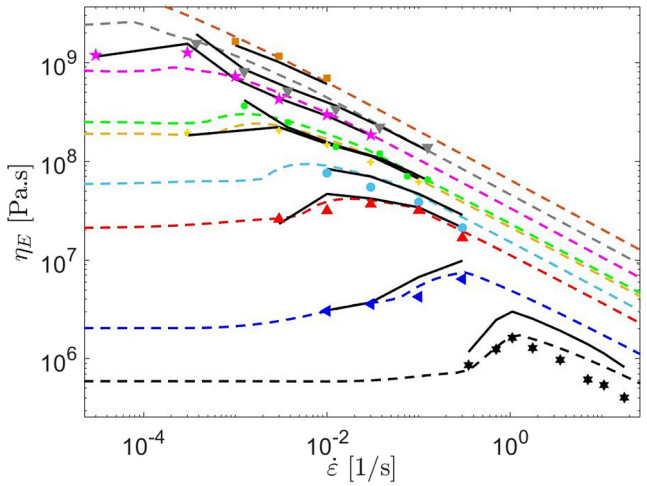

FIG. 16. Steady-state elongational viscosity versus elongational rate. Comparison between experimental data (o) of PS545 (■), PS390 (▼), PS285 (*), PS200 (●), PS185 (+), PS133 (●), PS100 (▲), PS50 (◀), and PS27 (*) at $T-T_g=23.4$ °C, and theoretical predictions based on the simplified TMA (dashed colored lines) and theoretical predictions based on the modified ML model (continuous black lines).

$$\eta_E(\dot\varepsilon)=\lim_{t\to\infty}\frac{3G_N^0}{\dot\varepsilon}\int_{x=0}^1(S_{zz}(x,t)-S_{rr}(x,t))\frac{d\varphi(x)\Phi(x)}{dx}dx,$$
$$\approx\frac{3G_N^0}{\dot\varepsilon}\lambda^2\int_{x=0}^1\left[\lim_{t\to\infty}S_{zz}(x,t)-S_{rr}(x,t)\right]dx$$
$$=\frac{3G_N^0}{\dot\varepsilon}\lambda^2\int_{x=0}^1\frac{\tau_x\dot\varepsilon}{2}dx, \quad \text{(C13)}$$

which gives in the limit of $\tau_x\dot\varepsilon/2\gg 1$,

$$\eta_E(\dot\varepsilon)\to_{\frac{\tau_x\dot\varepsilon}{2}\gg 1}\frac{3}{\dot\varepsilon}G_N^0\lambda^2. \quad \text{(C14)}$$

Likewise, Eq. (23) of the TMA expressed in the limit of a stretched chain leads to

$$\eta_E(\dot\varepsilon)=\int_0^\infty 3\,G_N^0\,\varphi(t)\Phi_C(t)\,\Phi_{\text{eff},\dot\varepsilon}(t)\,dt$$
$$\sim\int_0^\infty 3\,G_N^0\,\varphi(t)e^{-t\dot\varepsilon}\lambda^2dt=\frac{3}{\dot\varepsilon}G_N^0\lambda^2\sum_x\frac{\dot\varepsilon\tau_x}{1+\tau_x\dot\varepsilon}dx, \quad \text{(C15)}$$

which gives in the limit of $\tau_x\dot\varepsilon\gg 1$,

$$\eta_E(\dot\varepsilon)\to_{\tau_x\dot\varepsilon\gg 1}\frac{3}{\dot\varepsilon}G_N^0\lambda^2. \quad \text{(C16)}$$

This explains why in Fig. 16 both the simplified TMA and the modified ML model give similar results for the extensional viscosity $\eta_E(\dot\varepsilon)$, apart for low molar masses samples. As already mentioned, this is due to the chain end correction taken into account in Eq. (42), in the modified ML model.

REFERENCES

[1] Doi, M., *Introduction to Polymer Physics* (Oxford Science Publications, Oxford, 1995).

[2] Dealy, J. M., and R. G. Larson, *Structure and Rheology of Molten Polymers* (Hanser, Munich, 2006).
[3] Watanabe, H., "Viscoelasticity and dynamics of entangled polymers," Prog. Polym. Sci. **24**, 1253–1403 (1999).
[4] van Ruymbeke, E., C. Y. Liu, and C. Bailly, "Quantitative tube model predictions for the linear viscoelasticity of linear polymers," Rheol. Rev. **2007**, 53–134.
[5] Likhtman, A. E., and T. C. B. McLeish, "Quantitative theory for linear dynamics of linear entangled polymers," Macromolecules **35**, 6332–6343 (2002).
[6] McLeish, T. C. B., "Tube theory of entangled polymer dynamics," Adv. Phys. **51**, 1379–1527 (2002).
[7] Read, D. J., K. Jagannathan, S. K. Sukumaran, and D. Auhl, "A full-chain constitutive model for bidisperse blends of linear polymers," J. Rheol. **56**(4), 823–873 (2012).
[8] Doi, M., and S. F. Edwards, *The Theory of Polymer Dynamics*, International Series of Monographs on Physics (Oxford University, Oxford, 1986).
[9] Khaliullin, R. N., and J. D. Schieber, "Application of the slip-link model to bidisperse systems," Macromolecules **43**, 6202–6212 (2006).
[10] Masubuchi, Y., H. Watanabe, G. Ianniruberto, F. Greco, and G. Marrucci, "Comparison among slip-link simulations of bidisperse linear polymer melts," Macromolecules **41**, 8275–8280 (2008).
[11] Masubuchi, Y., J. I. Takimoto, K. Koyama, G. Ianniruberto, G. Marrucci, and F. J. Greco, "Brownian simulations of a network of reptating primitive chains," Chem. Phys. **115**, 4387–4394 (2001).
[12] Shivokhin, M. E., E. van Ruymbeke, C. Bailly, D. Kouloumasis, N. Hadjichristidis, and A. E. Likhtman, "Understanding constraint release in star/linear polymer blends," Macromolecules **47**, 2451–2463 (2014).
[13] Likhtman, A. E., S. K. Sukumaran, and J. Ramirez, "Linear viscoelasticity from molecular dynamics simulation of entangled polymers," Macromolecules **40**, 6748–6757 (2007).
[14] Yaoita, T., T. Isaki, Y. Masubuchi, H. Watanabe, G. Ianniruberto, and G. Marrucci, "Primitive chain network simulation of elongational flows of entangled linear chains: Role of finite chain extensibility," Macromolecules **44**, 9675–9682 (2011).
[15] Huang, Q., L. Hengeller, N. J. Alvarez, and O. Hassager, "Bridging the gap between polymer melts and solutions in extensional rheology," Macromolecules **48**, 4158–4163 (2015).
[16] Costanzo, S., Q. Huang, G. Ianniruberto, G. Marrucci, O. Hassager, and D. Vlassopoulos, "Shear and extensional rheology of polystyrene melts and solutions with the same number of entanglements," Macromolecules **49**, 3925–3935 (2016).
[17] Ianniruberto, G., G. Marrucci, and Y. Masubuchi, "Melts of linear polymers in fast flows," Macromolecules **53**, 5023–5033 (2020).
[18] Bach, A., K. Almdal, H. K. Rasmussen, and O. Hassager, "Elongational viscosity of narrow molar mass distribution polystyrene," Macromolecules **36**, 5174–5179 (2003).
[19] Ya, M. A., and C. J. S. Petrie, "Some conditions for rupture of polymer liquids in extension," J. Rheol. **41**, 1–25 (1997).
[20] Ianniruberto, G., and G. Marrucci, "A simple constitutive equation for entangled polymers with chain stretch," J. Rheol. **45**, 1305–1318 (2001).
[21] Marrucci, G., and G. Ianniruberto, "Interchain pressure effect in extensional flows of entangled polymer melts," Macromolecules **37**, 3934–3942 (2004).
[22] Bhattacharjee, P. K., D. A. Nguyen, G. H. Mckinley, and T. Sridhar, "Extensional stress growth and stress relaxation in entangled polymer solutions," J. Rheol. **47**, 269–290 (2003).
[23] Bach, A., H. K. Rasmussen, and O. Hassager, "Extensional viscosity for polymer melts measured in the filament stretching rheometer," J. Rheol. **47**, 429–441 (2003).
[24] Nielsen, J. K., H. K. Rasmussen, O. Hassager, and G. H. McKinley, "Elongational viscosity of monodisperse and bidisperse polystyrene melts," J. Rheol. **50**, 453–476 (2006).
[25] Auhl, D., P. Chambon, T. C. B. McLeish, and D. J. Read, "Elongational flow of blends of long and short polymers: Effective stretch relaxation time," Phys. Rev. Lett. **103**, 136001 (2009).
[26] van Ruymbeke, E., E. B. Muliawan, G. Hatzikiriakos, T. Watanabe, A. Hirao, and D. Vlassopoulos, "Viscoelasticity and extensional rheology of model Cayley-tree polymers of different generations," J. Rheol **54**, 643–662 (2010).
[27] Nielsen, J. K., H. K. Rasmussen, M. Denberg, K. Almdal, and O. Hassager, "Nonlinear branch-point dynamics of multiarm polystyrene," Macromolecules **39**, 8844–8853 (2006).
[28] Lentzakis, H., C. Das, D. Vlassopoulos, and D. J. Read, "Pom-pom-like constitutive equations for comb polymers," J. Rheol. **58**, 1855–1875 (2014).
[29] Huang, Q., O. Mednova, H. K. Rasmussen, N. J. Alvarez, A. L. Skov, K. Almdal, and O. Hassager, "Concentrated polymer solutions are different from melts: Role of entanglement molecular weight," Macromolecules **46**, 5026–5035 (2013).
[30] Wingstrand, S. L., N. J. Alvarez, Q. Huang, and O. Hassager, "Linear and nonlinear universality in the rheology of polymer melts and solutions," Phys. Rev. Lett. **115**, 078302 (2015).
[31] Wang, S. Q., *Nonlinear Polymer Rheology: Macroscopic Phenomenology and Molecular Foundation* (Wiley, Hoboken, 2018).
[32] Wagner, M. H., S. Kheirandish, and O. Hassager, "Quantitative prediction of transient and steady-state elongational viscosity of nearly monodisperse polystyrene melts," J. Rheol. **49**, 1317–1327 (2005).
[33] Wagner, M. H., "Scaling relations for elongational flow of polystyrene melts and concentrated solutions of polystyrene in oligomeric styrene," Rheol. Acta **53**, 765–777 (2014).
[34] Wagner, M. H., "An extended interchain tube pressure model for elongational flow of polystyrene melts and concentrated solutions," J. Non-Newtonian Fluid Mech. **222**, 121–131 (2015).
[35] Wagner, M. H., E. Narimissa, and V. H. Rolon-Garrido, "From melt to solution: Scaling relations for concentrated polystyrene solutions," J. Rheol. **59**, 1113–1130 (2015).
[36] Narimissa, E., and M. H. Wagner, "A hierarchical multi-mode molecular stress function model for linear polymer melts in extensional flows," J. Rheol. **60**, 625–636 (2016).
[37] Narimissa, E., and M. H. Wagner, "Modelling nonlinear rheology of unentangled polymer melts based on a single integral constitutive equation," J. Rheol **64**, 129–140 (2020).
[38] van Ruymbeke, E., J. Nielsen, and O. Hassager, "Linear and nonlinear viscoelastic properties of bidisperse linear polymers: Mixing law and tube pressure effect," J. Rheol. **54**, 1155–1172 (2010).
[39] Ianniruberto, G., A. Brasiello, and G. Marrucci, "Simulations of fast shear flows of PS oligomers confirm monomeric friction reduction in fast elongational flows of monodisperse PS melts As indicated by rheooptical data," Macromolecules **45**, 8058– 8066(2012).
[40] Yaoita, T., T. Isaki, Y. Masubuchi, H. Watanabe, G. Ianniruberto, and G. Marrucci, "Primitive chain network simulation of elongational flows of entangled linear chains: Stretch/orientation-induced reduction of monomeric friction," Macromolecules **45**, 2773– (2012).
[41] Ianniruberto, G., "Extensional flows of solutions of entangled polymers confirm reduction of friction coefficient," Macromolecules **48**, 6306–6312 (2015).
[42] Ianniruberto, G., and G. Marrucci, "Molecular dynamics reveals a dramatic drop of the friction coefficient in fast flows of polymer melts," Macromolecules **53**, 2627–2633 (2020).

[43] Matsumiya, Y., and H. Watanabe, "Non-Universal features in uniaxially extensional rheology of linear polymer melts and concentrated solutions: A review," Prog. Polym. Sci. **112**, 101325 (2021).

[44] Park, G. W., and G. Ianniruberto, "Flow-induced nematic interaction and friction reduction successfully describe PS melt and solution data in extension startup and relaxation," Macromolecules **50**, 4787–4796 (2017).

[45] Huang, Q., N. J. Alvarez, Y. Matsumiya, H. K. Rasmussen, H. Watanabe, and O. Hassager, "Extensional rheology of entangled polystyrene solutions suggests importance of nematic interactions," ACS Macro Lett. **2**, 741–744 (2013).

[46] O'Connor, T. C., N. J. Alvarez, and M. O. Robbins, "Relating chain conformations to extensional stress in entangled polymer melts," Phys. Rev. Lett. **121**, 047801 (2018).

[47] Bobbili, S. V., and S. T. Milner, "Chain tension reduces monomer friction in simulated polymer melts," J. Rheol. **64**, 1373–1378 (2020).

[48] Matsumiya, Y., Y. Masubuchi, H. Watanabe, Q. Huang, and O. Hassager, "Nonlinear elongational rheology of unentangled polystyrene and poly(p-tert-butylstyrene) melts," Macromolecules **51**(23), 9710–9729 (2018).

[49] Morelly, S. L., L. Palmese, H. Watanabe, and N. J. Alvarez, "Effect of finite extensibility on nonlinear extensional rheology of polymer melts," Macromolecules **52**, 915–922 (2019).

[50] Schweizer, S., and D. M. Sussman, "A force-level theory of the rheology of entangled rod and chain polymer liquids. I. Tube deformation, microscopic yielding, and the nonlinear elastic limit," J. Chem. Phys. **145**, 214903 (2016).

[51] Desai, P. S., and R. G. Larson, "Constitutive model that shows extension thickening for entangled solutions and extension thinning for melts," J. Rheol. **58**, 255–279 (2014).

[52] Doi, M., and S. F. Edwards, "Dynamics of rod-like macromolecules in concentrated solution," J. Chem. Soc., Faraday Trans. **274**, 560–570 (1978).

[53] Shchetnikava, V., J. Slot, and E. van Ruymbeke, "Comparative analysis of different tube models for linear rheology of monodisperse linear entangled polymers," Polymers **11**(5), 754–784 (2019).

[54] van Ruymbeke, E., D. Vlassopoulos, M. Kapnistos, C. Y. Liu, and C. Bailly, "Proposal to solve the time-stress discrepancy of tube models," Macromolecules **43**, 525–531 (2010).

[55] van Ruymbeke, E., C. Bailly, R. Keunings, and D. Vlassopoulos, "A general methodology to predict the linear rheology of branched polymers," Macromolecules **39**(18), 6248–6259 (2006).

[56] Colby, R. H., D. C. Boris, W. E. Krause, and S. Dou, "Shear thinning of unentangled flexible polymer liquids," Rheol. Acta **46**(5), 569–575 (2007).

[57] Parisi, D., J. Ahn, T. Chang, D. Vlassopoulos, and M. Rubinstein, "Stress relaxation in symmetric ring-linear polymer blends at Low ring fractions," Macromolecules **53**(5), 1685–1693 (2020).

[58] McLeish, T. C. B., and R. G. Larson, "Molecular constitutive equation for a class of branched polymers: The pom-pom polymer," J. Rheol. **42**, 81 (1998), 413-427.

[59] Wingstrand, S., M. van Drongelen, K. Mortensen, R. S. Graham, Q. Huang, and O. Hassager, "Influence of extensional stress overshoot on crystallization of LDPE," Macromolecules **50**(3), 1134–1140 (2017).

[60] Watanabe, H., Y. Matsumiya, and T. Sato, "Revisiting nonlinear flow behavior of rouse chain: Roles of FENE, friction-reduction, and Brownian force intensity variation," Macromolecules **54**, 3700–3715 (2021).

[61] Qin, J., and S. T. Milner, "Tube diameter of oriented and stretched polymer melts," Macromolecules **46**, 1659–1672 (2013).

[62] Pincus, P., "Excluded volume effects and stretched polymer chains," Macromolecules **9**(3), 386–388 (1976).

[63] Shahid, T., C. Clasen, F. Oosterlinck, and E. van Ruymbeke, "Diluting entangled polymers affects transient hardening but not their steady elongational viscosity," Macromolecules **52**(6), 2521–2530 (2019).

[64] Shahid, T., Q. Huang, F. Oosterlinck, C. Clasen, and E. van Ruymbeke, "Dynamic dilution exponent in monodisperse entangled polymer solutions," Soft Matter **13**(1), 269–282 (2017).

[65] Liu, C. Y., J. He, R. Keunings, and C. Bailly, "New linearized relation for the universal viscosity–temperature behavior of polymer melts," Macromolecules **39**, 8867–8869 (2006).

[66] van Ruymbeke, E., Y. Masubuchi, and H. Watanabe, "Effective value of the dynamic dilution exponent in bidisperse linear polymers: From 1 to 4/3," Macromolecules **45**(4), 2085–2098 (2012).

[67] van Ruymbeke, E., V. Shchetnikava, Y. Matsumiya, and H. Watanabe, "Dynamic dilution effect in binary blends of linear polymers with well-separated molecular weights," Macromolecules **47**, 7653–7665 (2014).

[68] Sato, T., Y. Kwon, Y. Matsumiya, and H. Watanabe, "A constitutive equation for Rouse model modified for variations of spring stiffness, bead friction, and Brownian force intensity under flow," Phys. Fluids **33**, 063106 (2021).

[69] Schwarzl, F., "Higher approximation methods for the relaxation spectrum from static and dynamic measurements of visco-elastic materials," Appl. Sci. Res. **2**(A4), 127–141 (1953).

[70] Shchetnikava, V., J. J. M. Slot, and E. van Ruymbeke, "A comparison of tube model predictions of the linear viscoelastic behavior of symmetric star polymer melts," Macromolecules **47**(10), 3350–3361 (2014).

[71] Lentzakis, H., S. Costanzo, D. Vlassopoulos, R. H. Colby, D. J. Read, H. Lee, T. Chang, and E. van Ruymbeke, "Constraint release mechanisms for H-polymers moving in linear matrices of varying molar masses," Macromolecules **52**(8), 3010–3028 (2018).

[72] Cox, W. P., and E. H. Merz, "Correlation of dynamic and steady viscosities," J. Polym. Sci. **28**, 619–622 (1958).

[73] Nielsen, J. K., H. K. Rasmussen, and O. Hassager, "Stress relaxation of narrow molar mass distribution polystyrene following uniaxial extension," J. Rheol. **52**, 885–899 (2008).

[74] Parisi, D., S. Costanzo, Y. Jeong, J. Ahn, T. Chang, D. Vlassopoulos, J. D. Halverson, K. Kremer, T. Ge, M. Rubinstein, G. S. Grest, W. Srinin, and A. Y. Grosberg, "Nonlinear shear rheology of entangled polymer rings," Macromolecules **54**, 2511–2827 (2021).

[75] Taghipour, H., S. Costanzo, D. Vlassopoulos, E. van Ruymbeke, and L. Hawke, "Entangled linear polymers in fast shear flows: Comparison of tube-model predictions and experimental data," J. Rheol. **65**, 1111–1137 (2021).

[76] Marrucci, G., "Dynamics of entanglements: A nonlinear model consistent with the Cox-Merz rule," J. Non-Newtonian Fluid Mech. **62**, 279–289 (1996).

[77] Mead, D. W., R. G. Larson, and M. Doi, "A molecular theory for fast flows of entangled polymers," Macromolecules **31**, 7895–7914 (1998).

[78] Wagner, M. H., and V. H. Rolon-Garrido, "The interchain pressure effect in shear rheology," Rheol. Acta **49**(5), 459–471 (2010).

[79] Marrucci, G., "Relaxation by reptation and tube enlargement: A model for polydisperse polymers," J. Polym. Sci. Polym. Phys. Ed. **23**, 159–177 (1985).

[80] Blackwell, R. J., O. G. Harlen, and T. C. B. McLeish, "Theoretical linear and nonlinear rheology of symmetric treelike polymer melts," Macromolecules **34**, 2579–2596 (2001).

[81] André, A., T. Shahid, F. Oosterlinck, C. Clasen, and E. van Ruymbeke, "Investigating the transition between polymer melts and solutions in nonlinear elongational flow," Macromolecules **54**, 2797–2810 (2021).